Synthesis and Characterization of Nickel Manganese Oxysulfide (NiMnOS) Catalyst for Reduction of Methylene Blue Dye in Aqueous Solution

Abraham Solomon Kasa

A Thesis Submitted to

The Department of Materials Science and Engineering

School of Mechanical, Chemical, and Materials Engineering

Presented in Partial Fulfillment of the Requirement for the Degree of Master's in Materials Science and Engineering

Office of Graduate Studies
Adama Science and Technology University

June 2022
Adama, Ethiopia

Synthesis and Characterization of Nickel Manganese Oxysulfide (NiMnOS) Catalyst for Reduction of Methylene Blue Dye in Aqueous Solution

Mr. Abraham Solomon Kasa

Advisor: Osman Ahmed Zelekew, Ph.D.

Co-advisor: Dinsefa Mensure Andoshe, Ph.D.

A Thesis Submitted to
The Department of Materials Science and Engineering

School of Mechanical, Chemical, and Materials Engineering,

Presented in Partial Fulfillment of the Requirement for the Degree of Master's in Material Science and Engineering

Office of Graduate Studies
Adama Science and Technology University

June 2022
Adama, Ethiopia

DECLARATION

I hereby declare that this Master Thesis entitled “Synthesis and Characterization of Nickel Manganese Oxysulfide (NiMnOS) Catalyst for Reduction of Methylene Blue Dye in Aqueous Solution” is my original work. That is, it has not been submitted for the award of any academic degree, diploma, or certificate in any other university. All sources of materials that are used for this thesis have been duly acknowledged through citation.

_____	_____	_____
Name of the Student	Signature	Date

RECOMMENDATION

I/we, the advisor(s) of this thesis, hereby certify that I/we have read the revised version of the thesis entitled "Synthesis and Characterization of Nickel Manganese Oxysulfide (NiMnOS) Catalyst for Reduction of Methylene Blue Dye in Aqueous Solution" prepared under my/our guidance by Abraham Solomon Kasa submitted in partial fulfillment of the requirements for the degree of Master's of Science in Materials Science and Engineering

Therefore, I/we recommend the submission of revised version of the thesis to the department following the applicable procedures.

_____	_____	_____
Major Advisor	Signature	Date
_____	_____	_____
Co-advisor	Signature	Date

APPROVAL PAGE

I/we, the advisors of the thesis entitled "Synthesis and Characterization of Nickel Manganese Oxysulfide (NiMnOS) Catalyst for Reduction of Methylene Blue Dye in Aqueous Solution" and developed by Abraham Solomon Kasa hereby certify that the recommendation and suggestions made by the board of examiners are appropriately incorporated into the final version of the thesis.

Major Advisor	Signature	Date
Co-advisor	Signature	Date

We, the undersigned, members of the Board of Examiners of the thesis by Abraham Solomon Kasa have read and evaluated the thesis entitled "Synthesis and Characterization of Nickel Manganese Oxysulfide (NiMnOS) Catalyst for Reduction of Methylene Blue Dye in Aqueous Solution" and examined the candidate during the open defense. This is, therefore, to certify that the thesis is accepted for partial fulfillment of the requirement of the degree of Master of Science in Material science and engineering.

Chairperson	Signature	Date
Internal Examiner	Signature	Date
External Examiner	Signature	Date

Finally, approval and acceptance of the thesis are contingent upon the submission of its final copy to the Office of Postgraduate Studies (OPGS) through the Department Graduate Council (DGC) and School Graduate Committee (SGC).

Department Head	Signature	Date
School Dean	Signature	Date
Office of Postgraduate Studies,	Dean Signature	Date

ACKNOWLEDGEMENT

I would like to express my deep gratitude to Dr. Osman Ahmed, my research advisor, for his patient guidance, enthusiastic encouragement, and useful critiques of this research work. I would like to express my gratitude to Dr. Dinsefa Mensure, my co-advisor, for his valuable advice and insightful comments. My grateful thanks are also extended to Mr. Demeke Tesfaye and all staff members of the Materials Science and Engineering department. I would like to thank Adama Science and Technology University for providing this Masters scholarship and funding the research work under the number ASTU/SM-R/437/22. Finally, I wish to thank my parents for their support and encouragement throughout my study.

TABLE OF CONTENTS

LIST OF TABLES

LIST OF FIGURES

LIST OF ACRONYMS

AB Azure B

AC Activated Carbon

AO Auramine O

BET Brunauer-Emmett-teller

BG Brilliant Green

BR Basic Red 2

4-CC 4-chlorocatchol

CV Crystal Violet

EDS Energy-Dispersive X-ray spectroscopy

HEP Hydrogen Evolved Photocatalyst

MB Methylene Blue

MG Malachite Green

MO Methylene Orange

MV Methyl Violet

NR Neutral Red

PDS Peroxydisulfate

PVP Polyvinylpyrrolidone

RHB Rhodamine B

SEM Scanning Electron Microscope

XDS Energy dispersive x-ray Spectroscopy

XPS X-ray Photoelectron Spectroscopy

XRD X-ray Diffractometer

GC-MS Gas Chromatography Mass Spectrometry

BET Brunauer-Emmett-Teller

ABSTRACT

Environmentally toxic organic dyes discharged from industries as wastes are a great public concern due to their harsh effect on humans and aquatic organisms even at low concentrations. As a result, effective removal and/or reduction of these toxic substances is very critical. Bimetal oxysulfide catalysts have been widely used for reduction of organic dyes due to their facile preparation technique and effective catalytic performance. However, toxic hydrazine is used as a reducing agent during the preparation process. In this study, noble metal free flower-like nickel manganese oxysulfide (NiMnOS) catalysts were produced via a facile and environmentally friendly approach. The NiMnOS catalysts were synthesized by varying Ni: Mn molar ratios (Ni: Mn = 25:75, 50:50, 75:25 and assigned as NiMnOS-25, NiMnOS-50, and NiMnOS-75, respectively) at low synthesis temperature of 90 °C in a water bath. The bare NiOS and MnOS were also prepared with the same technique for comparison. The prepared samples were characterized using X-ray Diffractometer (XRD), X-ray photoelectron spectroscopy (XPS), Scanning electron microscope (SEM), Energy-dispersive X-ray spectroscopy (EDS), Fourier transforms infrared spectroscopy (FTIR), and UV–Vis spectroscopy to determine phase purity, chemical binding, and ionization state, the morphology and composition of the particles, functional groups, and optical property of samples, respectively. The catalytic activity of the samples was investigated through the reduction of methylene blue (MB) dye in the presence of $NaBH_4$ in an aqueous solution. The NiMnOS-25 catalyst exhibited excellent performance and reduced 98.46% of 10 ppm methylene blue (MB) solution within 5 min. However, NiOS, NiMnOS-50, NiMnOS-75, and MnOS were reduced 9.6%, 98.41%, 97.04%, and 6.40% of MB dye solution, respectively, within 7 min. The catalytic reduction activity could be mainly attributed to the synergistic effect between the two metals (Ni and Mn), more exposed active sites, and the optimum amount of Mn in the NiMnOS sample. The recyclability of catalyst was performed for four runs and good stability and durability were obtained. Finally, a possible mechanism for methylene blue (MB) dye reduction reaction was proposed. Therefore, NiMnOS could be a good candidate for the reduction of organic dyes in environmental remediation.

Key words: *Bimetal Oxysulfide, NiMnOS catalyst, Reduction, catalytic efficiency, Methylene blue.*

CHAPTER ONE

1. Introduction

1.1 Background of the Study

Water is a fundamental resource that ensures the survival of all living things on the earth. Fresh and readily available water has of outmost relevance for life on earth and the development of the economy of one nation (Schellekens, Heidecke, Nguyen, & Spit, 2018). But, nowadays, access to clean and improved water is becoming a great pressing issue because of the increasing environmental pollution that results from the rapid growth of industrialization and urbanization (Fu, Cheng, & Lu, 2015). The major causes of water pollution are different kinds of organic and inorganic pollutants caused by various industrial wastes, and natural and anthropogenic factors (Quiton, Lu, & Huang, 2021). Inorganic contaminants are the compounds of inorganic by-products and persist longer in an aqueous system, don't degrade easily, and cause further deterioration. Fluoride, halide, iron, nitrate, arsenic, heavy metals, etc. are the common inorganic pollutants of water (Srivastav & Ranjan, 2020). Organic contaminants include different compounds of pesticides, veterinary products, pharmaceuticals, personal care products, industrial compounds/by-products, engineered nanomaterials, food additives, and organic dyes (Mahmood, Momin, Ali, Naeem, & Khan, 2022).

Synthetic organic dyes and pigments discharged by industries such as textiles, paints, printing inks, cosmetics, plastics, and paper cause significant environmental pollution because of their hydrophilic nature, complex aromatic structure, and high stability against water, light, chemicals, temperature, and etc. (Y. Liu et al., 2018). In addition, they seriously affect human health and the environment due to their toxicity, long persistent, teratogenic, carcinogenic, and mutagenic properties (Abay, Kuo, Chen, & Saragih, 2017). Around 10% to 15% of the dye produced worldwide (over 800 000 tons per year) ends up in the environment, either as effluent or as a result of losses during the drying process (Rojas & Horcajada, 2020). Dyes are divided into acid, basic, direct, disperse, mordant, reactive, sulfur, azoic, and vat dyes based on their solubility, chemical properties, and/or role in the textile industry (Rojas & Horcajada, 2020).

Methylene blue (3,7 bis(dimethylamino) phenothiazine-5-ium chloride), a heterocyclic aromatic dye, is an important basic dye (Y. Liu et al., 2018). Methylene blue (MB) is

categorized as a cationic thiazine dye used for printing calico, dyeing cotton, and dyeing leather. It is also widely used in the textile industry as well as in biological materials as a photodynamic antimicrobial reagent (Senobari & Nezamzadeh-Ejhieh, 2018; Sohrabnezhad, Pourahmad, Rakhshaee, Radaee, & Heidarian, 2010). When this toxic MB is excessively interred into the human body, it can cause serious ailments such as central nervous system toxicity, gastrointestinal infections, and decolorization of the brain parenchyma, due to inhibition of oxidase enzymes in the body (Begum et al., 2020). It can also induce eye burns, gastrointestinal tract irritation, and skin irritation.

Thus far, various strategies such as biological process (aerobic and anaerobic degradation), physical/traditional process (adsorption, membrane filtration, and flocculation), and chemical process (photocatalytic degradation, ozonation, Fenton like reaction, electrochemical and photochemical oxidation) have been developed and employed for such dye-containing waste water (Ba-Abbad, Kadhum, Mohamad, Takriff, & Sopian, 2012; Hao Chen, Zhong, Wu, Zhao, & Yan, 2012; H. Hu et al., 2015; X.-y. Li, Cui, Feng, Xie, & Gu, 2005; Pandya, Pandya, & Dave, 2018; Zagklis, Koutsoukos, & Paraskeva, 2012). However, several constraints, such as discharge of massive amounts of sludge, low efficiency of dye removal, expensive recycling steps, release of non-degradable and toxic byproducts into the environment, slow process, higher cost of materials, etc., limit the practical utility of this technique (Abay, Kuo, et al., 2017; Al-Khalid & El-Naas, 2012; Bokare, Chikate, Rode, & Paknikar, 2008; Manu & Chaudhari, 2002).

The catalytic reduction of organic dye molecules is the most advanced technique due to several reasons (Begum et al., 2020). It is an easy operation, high efficiency, and low-cost process. In addition, harmful dyes are converted to useful byproducts that can be employed as precursors or raw materials in a variety of industries (Kong, Zhu, Chen, Huang, & Chen, 2017). This technique is not only a quick process, but it also achieves total dye removal, making it preferable to the oxidative degradation process, which only achieves incomplete dye removal. Furthermore, the recycling procedures for the catalysts used for reduction reactions are simple and straightforward (Swathi & Buvaneswari, 2008). The recycling of the utilized catalyst from the reaction media in the reduction reaction is usually accomplished using centrifugation (Zelekew, Kuo, & Abdullah, 2019). This also suggests that the catalytic reduction is more cost-effective than the conventional adsorption technique, which requires lengthy separation procedures and additional setups to remove the adsorbed dye from the catalyst (Najeeb, Ahmad, Nazir, Naseem, & Kanwal, 2021).

The catalytic reductive degradation of organic dyes in the presence of sodium borohydride ($NaBH_4$) occurs by the electron transfer mechanism (Kassem, Abdelhamid, Fouad, & Ibrahim, 2021). In the absence of an effective catalyst, the reduction of dye is thermodynamically favorable, but there is a significant kinetic barrier between the electron donor BH_4^- ion and acceptor dyes, which might obstruct the electron transport (Hashimi, Nohan, Chin, Zakaria, & Chia, 2019). The catalysts, surprisingly, are capable of reducing the potential difference due to their high Fermi potentials, which allow them to degrade dyes efficiently (Saikia, Miah, & Das, 2017). As a result, designing and synthesizing catalytic materials with appropriate redox potential between the electron donor and acceptor species to operate as an efficient electron relay system is very crucial (Saikia et al., 2017).

Catalysts can be categorized as homogeneous and/or heterogeneous catalysts. Homogeneous catalyst is not highly developed for wastewater treatment because it involves the use of a liquid phase catalyst (Maocong Hu, Liu, Yao, Ma, & Wang, 2018). It is also difficult to separate the catalyst technically and/or economically as well as the dissolved catalyst can result in environmental problems. A heterogeneous catalyst involves the use of solid materials as a catalyst, and the separation of the catalyst is also not difficult (Marcì & Palmisano, 2019). In addition, a solid catalyst (usually metal or metal on support) of a small amount can speed up the chemical reaction and efficiently degrade water pollutants.

To date, several catalysts have been produced for the removal of such pollutants, including zeolites, noble metal nanoparticles such as Au, Ag, Pt, Pd, metal oxides, ferrites, and composite materials (C. Singh, Goyal, & Singhal, 2014). Noble metal nanoparticles are well-known catalysts in the reduction reactions and have piqued the interest of researchers for a long time due to their effective catalytic activity, however, the high manufacturing costs of these materials limit their usage as catalysts in large-scale applications (Benhadria et al., 2022). Thus, the investigation of inexpensive, environmentally friendly, and efficient catalysts is still the main concern for researchers (H. Sun et al., 2019b).

Bimetallic catalysts have better catalytic potential than their individual metal (monometallic equivalents), because of the synergistic effects between two metals and the degree of freedom that may be modified to boost the catalytic efficiency of bimetallic nanomaterials (Naz et al., 2021). The increased efficiency of the bimetallic catalyst is commonly related to the electronic interactions between the two metals at the metal/metal interfaces. One metal will attract electrons from the active species, causing its d-electron density to change and facilitating effective catalysis (Alshammari, 2018). The interatomic distances between the

metal atoms can be changed by changing the properties of the electron orbitals, which is significant in improving catalytic efficiency and leading to enhanced catalysis compared to metal nanoparticles (Alshammari, 2018).

Nowadays, bimetallic oxysulfide catalysts have been employed for the treatment of water pollutants due to their facile, green, and economic preparation technique, and effective catalytic performance. Abdeta A. B. et al. (Abdeta et al., 2021) Synthesized a novel AgMoOS oxysulfide catalysts and effectively reduced chromium (VI) and organic dyes such as methylene blue, methyl orange, Rhodamine blue, and 4-nitrophenol under dark conditions. Wu Q. et al. (Q. Wu et al., 2021) synthesized a wool-coiled MoSrOS oxysulfide catalyst for the reduction of heavy metal ions and organic pollutants. Jiang L. et al. (L. Jiang, Li, Wu, & Zhang, 2021) prepared oxygen vacancy-rich bismuth oxysulfide (Bi_2O_2S) for effective photocatalytic reduction of CO_2 to CH_4 under visible light irradiation. Re J. et al. (Ren, Jiang, Li, & Zhang, 2021) synthesized cobalt-doped bismuth oxysulfide (Co-doped Bi_2O_2S) for catalytic degradation of tetracycline through peroxymonosulfate activation. Tadesse S. F. et al. (Tadesse, Kuo, Kebede, & Duresa, 2020a) synthesized vanadium-doped $Mo(O,S)_2$ oxysulfide for enhanced photocatalytic degradation of methylene blue dye under visible light irradiation. Tadesse S. F. et al. (Tadesse, Kuo, Kebede, & Wolde, 2021) also synthesized $Nd_2O_3/Mo(S,O)_{3-x}{\cdot}0.34H_2O$ heterojunction for efficient photocatalytic degradation of rhodamine blue, methylene blue, and methylene orange. Nishioka S. et al. (Nishioka et al., 2019) synthesized zinc-based oxysulfide $SrZn_2S_2O$ photocatalyst for reduction and oxidation of water under bandgap irradiation. Abdullah H. et al. (Abdullah, Gultom, & Kuo, 2017) prepared indium oxysulfide nanosheet ($In_2(O,S)_3$ NS) photocatalyst to reduce toxic hexavalent chromium and produce hydrogen under halogen and Xe lamp illumination. However, there were no works reported on the synthesis of bimetal nickel manganese oxysulfide (NiMnOS) catalyst prepared in a water bath at 90 °C for reduction of MB dye.

In this study, the novel flower-like nickel manganese oxysulfide (NiMnOS) was synthesized for the reduction of methylene blue (MB) dye in an aqueous solution. We designed to synthesize the catalyst in a water bath and toxic hydrazine is not used in the process. The catalyst was prepared by varying amounts of Ni and Mn molar ratio added into the solution. For comparison purpose, bare NiOS and MnOS were also synthesized and tested for reduction of MB. The reduction reaction of methylene blue (MB) with the catalyst and sodium borohydride was conducted at room temperature. The NiMnOS-25 catalyst showed

the highest catalytic activity among all the prepared samples. The characteristics of the catalyst, the degradation performance, stability and reusability, and the mechanism of catalytic reaction were studied. This research helps to inspire the development of environmentally friendly, effective, and recyclable catalysts, as well as increase the applicability of catalysts in environmental remediation.

1.2 Statement of the Problem

Over the past few decades, organic dyes discharged into the environment mainly in water bodies are rapidly growing due to the expansion of industries. As a result, effective removal and/or reduction of these toxic substances is very critical. In recent years, a number of heterogeneous catalysts based on noble metals such as Ag, Au, Pd, and Pt have been developed and widely utilized for the reduction of organic dyes (Shultz et al., 2019). However, their expensive price and limited availability limit their use in practical applications (Nagarajan & Venkatanarasimhan, 2019). In addition, they require organic polymers as a carrier or stabilizing agent to prevent nanoparticle aggregation (Nagarajan & Venkatanarasimhan, 2019).

For this reason, bimetallic oxysulfide catalysts have attracted much interest due to their effective catalytic activity resulting from more degree of freedom, the synergistic effects between constituent metals, and more active sites for the reaction (Abay, Chen, & Kuo, 2017). However, oxysulfide catalysts are widely synthesized by using hydrazine as a reducing agent. Hydrazine is a very toxic chemical to humans because it is absorbed immediately via the skin and lungs, causing substantial damage to the kidneys, liver, lungs, and central nervous system (Samanta et al., 2020). The US Environmental Protection Agency (EPA) has classified hydrazine as a possible carcinogen, with a threshold limit value (TLV) of 10 parts per billion (K. Wang et al., 2021). Therefore, the preparation of catalysts with low cost, environmentally friendly, and effective catalytic activity at low processing temperature is still challenging. This work focused on the synthesis of bimetal oxysulfide NiMnOS catalyst for the reduction of methylene blue (MB) dye in an aqueous solution. The catalyst was prepared at a low temperature of 90 °C with a facile and environmentally friendly approach when compared with the conventional method which uses toxic hydrazine as a reducing agent. Therefore this work provides a catalyst with effective catalytic activity and ecofriendly preparation method.

1.3 General Objective

Synthesis and characterization of nickel manganese oxysulfide (NiMnOS) catalyst for reduction of methylene blue (MB) dye in an aqueous solution.

1.4 Specific Objectives

- Synthesizing bimetal NiMnOS catalyst with varying Ni: Mn molar ratios (Ni: Mn = 25:75, 50:50, 75:25) by a facile and ecofriendly technique using a water bath.
- Characterizing the prepared nickel manganese oxysulfide (NiMnOS) catalysts.
- Studying the catalytic activity, stability, and reusability of the catalysts

1.5 Significance of the Study

Developing efficient, low cost and eco-friendly methods for wastewater treatment is a very crucial activity due to the wide-scale discharge of pollutants and environmental changes which resulted from rapidly growing industrialization. This work primarily benefits the industries that discharge effluent with a high concentration of organic dyes such as textile, paper, cosmetic, and leather processing industries. Ethiopia has one of the most rapidly growing economies in the world and there is a lot of interest in the expansion of industry and agriculture. But, Ethiopia has a weak waste management system. Thus, water bodies are exposed to the released toxic wastes. This work is designed to prepare a bimetal NiMnOS catalyst that helps to reduce environmental pollution caused by the discharge of organic pollutants. It is not only to provide effective materials for the degradation of organic contaminants but also prevent pollution occurred during the synthesis process by providing a facile preparation technique at a lower temperature.

1.6 Scope of the Study

This study covered the preparation of bimetal NiMnOS oxysulfide catalyst by varying amounts of Ni and Mn precursor ratio. The catalyst was synthesized by simple and facile method in a water bath at a low synthesis temperature of 90 °C. The synthesized samples were characterized using XRD, XPS, EDS, SEM, FTIR, and UV-Vis spectrometer. The catalytic reduction performance of the samples was investigated by using methylene blue (MB) dye in an aqueous solution. The stability and reusability of the catalyst were also studied by repeating the degradation process for 4 runs. Finally, the proposed reduction

mechanism of the catalyst was explained. It is more focused on designing an eco-friendly synthesis of the catalyst for effective reduction of methylene blue dye in an aqueous solution.

CHAPTER TWO

2. Literature Review

2.1 Water Pollution

Water pollution is a major global concern because of its adverse consequences, such as ecosystem disruption and human life loss (Islam & Tanaka, 2004). Improper wastewater management from various sources, such as public service, domestic, system loss/leakage, and industrial wastes, are the major causes of water pollution. Among the other sources, Industrial wastewaters account for 42.4 percent of total volume, while home wastewater accounts for 36.4 percent (Saeed, Usman, & ul Haq, 2018). Industrial wastes are the primary causes of water pollution. Among all industrial wastes, textile wastes are the most harmful contaminant, depending on the amount and composition of effluents (Y. Wu, 2017). The major water pollutants discharged during industrial processing are dyes, which pose a serious threat to aquatic biota and ecosystems. Dyes are utilized in a variety of industries, including textiles, food, plastic, printing, leather, cosmetics, and pharmaceutics, all of which generate considerable amounts of dye-containing wastewater (B. Sun et al., 2018). Organic dyes' high toxicity not only causes a variety of diseases and ailments but also has an impact on the ecosystem, such as inhibiting the photosynthetic process in aquatic plants by obstructing sunlight and interfering with aquatic creatures' normal growth by lowering water oxygen capacity (Honarmand, Golmohammadi, & Naeimi, 2019). Hence, wastewater treatment before disposal is critical (Abdelbasir & Shalan, 2019).

Recently, efforts have been made to degrade organic contaminants by designing effective catalysts with regulated morphologies and structures. Among various constructed catalysts, nanostructure catalysts such as metal oxide, metal hydroxide, metal sulfide, metal oxysulfide, mixed compounds, etc. have received a lot of interest during the last decade due to their distinctive physical and chemical features (Ayodhya & Veerabhadram, 2018) such as high surface area, more exposed surface active sites, and superior electron transfer capabilities which gives them great advantages in catalysis (Jia et al., 2017).

2.2 Metal Oxide

Metal oxide catalysts have become important in most refining and petrochemical processes, in the synthesizing of specialized chemicals, and, more recently, in the improvement of environmental issues, in particular for the removal of pollutants by optimizing reaction selectivity to eliminate waste byproducts (Védrine, 2019). Recently, Nano-sized metal oxide catalysts have been widely used (especially in advanced oxidation processes) for the treatment of waste water and showed enhanced degradation performance since it displays excellent characteristic outcomes (Gnanasekaran et al., 2017).

Several metal oxides such as titanium dioxide (TiO_2), zinc oxide (ZnO), tungstate (WO_3), vanadate (VO_4), molybdate (MoO_4), etc. have been reported. Among them, TiO_2 is the most widely studied catalyst due to its high photocatalytic activity, low cost, chemical stability, and low toxicity (Chan, Yeong Wu, Juan, & Teh, 2011). Zinc oxide is another metal oxide catalyst used as an alternative material to TiO_2 with high photocatalytic activity, especially for the degradation of industrial wastes at neutral pH (Xiaogang Chen et al., 2010). TiO_2 and ZnO absorb solar radiation in the UV region, which accounts for just 5% of total solar energy and a minor portion of total solar radiation when compared to visible (43%) and infrared (52%) rays (Serrà et al., 2019). Despite this, they are affected by electron and hole recombination during irradiation (Lin, Lu, & Huang, 2019; Martínez-Vargas et al., 2019). To overcome this limitation, different modifications by using metals (e.g. transition metals, lanthanides, and noble metals), non-metals (e.g sulfur, carbon, phosphorus, and nitrogen), and supporting materials (cellulose, plants, activated carbon, etc.) have conducted (Chan et al., 2011; X. Li, Zhang, Wang, Wu, & Ma, 2021). In addition to metal oxides, metal hydroxides were also studied and utilized as a catalyst in the application of environmental remediation.

2.3 Metal Hydroxide

Transition metal hydroxide catalysts have been employed for the removal of pollutants from waste water as prospective noble metal free catalysts due to their abundant supplies, low cost, versatile structure, and good performance. Scientists recently designed and successfully constructed a well-defined hierarchical architecture made of ultrathin nanosheets, which is used to eliminate the agglomeration problem and increased stability while maintaining the ultrathin nanosheets' atomic-scale thickness and high surface area (Jia et al., 2017). It is used to enhance the performance of hydroxide catalysts toward waste water treatment. Metal

hydroxides such as $Ni(OH)_2$, and layered double hydroxide (LDH) have been widely utilized in water purification methods such as photo-catalysis and adsorption. $Ni(OH)_2$ occurs in two forms: α-$Ni(OH)_2$ and β-$Ni(OH)_2$. Both structures are hexagonal, with brucite-type layers either randomly stacked along the C-axis in (α-$Ni(OH)_2$) or well-ordered along the C-axis in (β-$Ni(OH)_2$) (Nagajyothi, Deyarayapalli, Tettey, Vattikuti, & Shim, 2019). $Ni(OH)_2$ has gained particular attention due to its low-cost, unique electrochemical characteristics (such as high specific capacitance), and ecologically benign property (Martínez-Sánchez, Regmi, Lee, & Rodríguez-González, 2021). Layered double hydroxide (LDH), inorganic layered materials with a hydrotalcite-like structure, attracted wide attention in advanced oxidation processes due to its unique structural advantages such as large surface area, massive active sites, interlayer ions exchange, and excellent stability (Zhao et al., 2018). Several LDH catalyst such as, Fe-Co LDH (Gong et al., 2017), Ni-Co LDH (L. Zhang, Yang, Zhou, Lin, & Zhou, 2022), Zn-Cr LDH (Mohapatra & Parida, 2012), Co-Mn LDH (Zhao et al., 2018), Co-Mg-Al LDH (Jawad, Lu, Chen, & Yin, 2014), etc. has been reported for removal of pollutants from waste water.

2.4 Metal Sulfide

Metal sulfides are compounds in which the sulfur anion reacts with a metal/semi-metal or cations to generate M_xS_y, giving monometallic stoichiometry of MS, M_2S, M_3S_4, and MS_2. Similarly, bi-metal sulfide is formed as $A_{1-x}B_xS_y$, (where x and y represent integers, A and B are different metals) (Chandrasekaran et al., 2019). Metal sulfides mainly transition metal sulfides (TMSs) are widely utilized in environmental protection and other application such as light-emitting devices, solar cells, energy storage, and conversion, etc. due to their better electrical conductivity, rich redox sites, excellent optical properties, superior mechanical and thermal stabilities, and strong catalytic performance than other commonly used transition metal catalysts (Y. Li et al., 2021).

Several TMS-based heterogeneous catalysts have been discovered for wastewater treatment in various Advanced oxidation processes such as electrochemical oxidation (Zheng, Teng, Ye, Zheng, & Fang, 2020), Fenton-like oxidation (Luo et al., 2020), and photocatalytic oxidation (Huerta-Flores, Torres-Martínez, Moctezuma, Singh, & Wickman, 2018) due to their capacity to absorb visible and/or UV light, narrow optical bandgaps, and charge transport properties, versatile redox nature, and strong electrical conductivity (Y. Li et al., 2021). The problems associated with metal sulfides are instability of nanostructures,

agglomeration of the particles, use of expensive equipment and time-consuming process, and use of toxic chemicals as reducing and capping agents (Munyai & Hintsho-Mbita, 2021). To overcome those limitations various strategies such as green synthesis method, doping with other metals, coupling them with other noble metals and carbon materials, etc. have been employed (Junaid et al., 2019; Mazaheri, Ghaedi, Asfaram, & Hajati, 2016; Pouretedal, Norozi, Keshavarz, & Semnani, 2009; Y. Wang et al., 2020).

2.5 Metal Oxysulfide

Metallic oxysulfide, which is synthetic and hardly available in nature, is a compound composed of metal, oxygen, and sulfur with negative oxidation states (e.g., –II) for both oxygen and sulfur (Larquet & Carenco, 2020). The generic formula for ternary oxysulfide is written as M*x*O*y*S*z*. Due to its negative oxidation state, sulfur forms no bounds with oxygen in oxysulfides in contrast to more common metal sulfates $M_x(S^{VI}O_4)_y$ where the sulfur is +VI (Eastman, Brewer, Bromley, Gilles, & Lofgren, 1951; Larquet & Carenco, 2020). Generally, a category of compounds that is independent of both metal sulfides and metal oxides represents a metal oxysulfide, however, common properties may be identified depending on the metal, the anion substitution, and the crystal structure. Oxysulfide compound was first observed by Mosander in 1827, who saw both sulfur and oxygen with metal in the process of sulfiding Ce_2O_3 into Ce_2S_3 using H_2S (Larquet & Carenco, 2020). He noticed the presence of oxygen and sulfur combined with the metal in a single product, along with the formation of cerium sulfate.

Since then, various oxysulfides were synthesized and utilized for different applications such as hydrogen evolutions, batteries, CO_2 reductions, sensors, and purification of water contaminants. Various research was reported on using oxysulfide-based catalysts for the treatment of organic and inorganic contaminants in wastewater. These catalysts have received the wide attention of researchers not only for their catalytic performance but also for their facile preparation technique.

2.6 Synthesis Method of Oxysulfide-based Catalyst

Oxysulfide-based catalyst is mainly synthesized using a co-precipitation technique at low processing temperature for the application of water remediation. In addition, co-precipitation on support was also used to enhance the property of nano-catalysts.

2.6.1 Co-precipitation

Oxysulfide-based catalysts are successfully synthesized by a co-precipitation method. In this process, metal precursors for the defined oxysulfide catalyst are dissolved into distilled water with vigorous stirring. After a certain number of minutes of stirring, a source of sulfur is added to the mixture and subjected to a reaction. Then, hydrazine is dropped and heated at 90 °C for an hours. Consequently, after cooling to room temperature the resulting precipitates are washed several times with water and ethanol. At the end, the obtained precipitates are dried in a rotary evaporator or oven.

Vanadium-doped bismuth oxysulfide catalysts are also synthesized by the same procedure mentioned above. A bismuth source precursor, $Bi(NO_3)_3 \cdot 5H_2O$ (10 mmol), is mixed with 65 mL of HNO_3 with continuous stirring and then deionized water is added to make a 300 mL solution. Then, 200 mL of (1 mmol) NH_4VO_3 and 100 mL of thioacetamide solution were dropped sequentially with stirring at room temperature for 20 min. The PH of the solution is adjusted by 1M NaOH to 6.5 with further stirring for 20 min. After the solution was heated at 90 °C for 4 hours under vigorous stirring, the obtained precipitate was cooled down to room temperature, washed with deionized water and ethanol, and dried (Abay, Kuo, et al., 2017). The preparation process is schematically described in Figure 2.1.

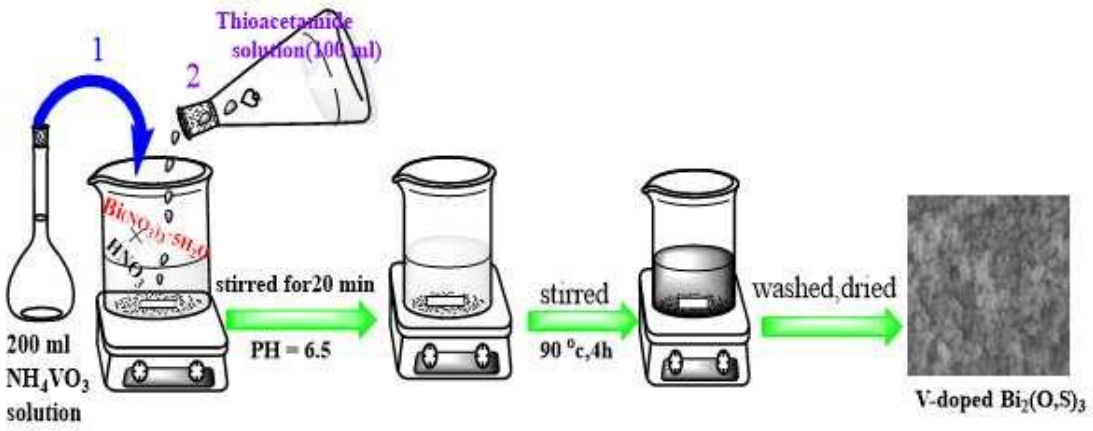

Figure 2.1. The schematic diagram for the synthesis of V-doped $Bi_2(O,S)_3$ catalyst (Abay, Kuo, et al., 2017)

The CuBiOS and CuOS nanoparticle catalysts were also prepared by the same technique with varying amounts of hydrazine (0.00, 0.15, and 0.45 mL) dropped into the solution mixture (Guo et al., 2020). The XRD analysis showed that the diffraction peaks position of

the prepared samples corresponded to the structure of CuS with a peak shift toward a smaller angle which is caused by the incorporation of a larger ionic radius Bi^{3+} (Bi^{3+} = 103 pm) into the crystal lattice of CuS. The addition of various amounts of N_2H_4 did not affect the position and intensity of CuBiOS diffraction peaks. However, the catalytic activity of the samples could be improved with the optimum amount of hydrazine. The results indicated that CuBiOS catalyst synthesized with 0.3 mL of N_2H_4 had the highest catalytic activity.

2.6.2 Co-precipitation on a Support

Oxysulfide-based catalyst can be prepared by precipitation on support. The CuVOS supported on porous silica was prepared as shown in Figure 2.2 (a) (H. Sun et al., 2020). The support, porous SiO_2, enhanced the catalytic activity by increasing surface area and reducing aggregation of the catalyst to facilitate better contact between the pollutant and catalyst. Thus, it is helpful to speed up the reaction and improve the catalytic efficiency of the catalyst.

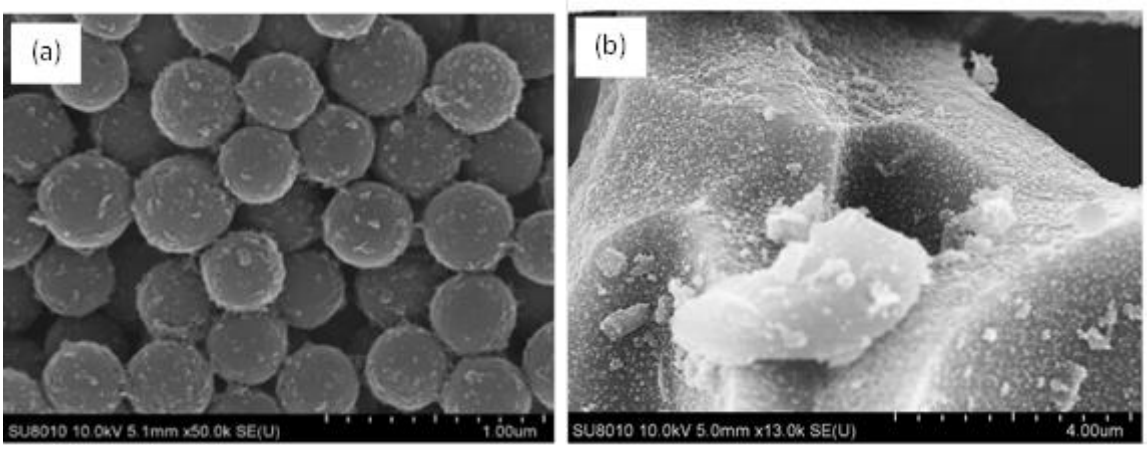

Figure 2.2. SEM image of (a) SiO_2 supported CuVOS and (b) activated carbon supported CuSnOS (H. Sun et al., 2021; H. Sun et al., 2020)

CuSnOS nanoparticle catalyst was also synthesized by a co-precipitation technique using activated carbon as a support for efficient catalytic reduction of organic dyes and heavy metals under dark conditions as shown in Figure 2.2 (b) (H. Sun et al., 2021). A high surface area, porous structure, and enriched surface chemistry with highly reactive surface functionality made the activated carbon utilized as catalyst support. Spherical CuSnOS nanoparticles were uniformly distributed on the surface of activated carbon to prevent agglomeration and enhanced the active site of the catalyst. Good stability and superior catalytic activity of CuSnOS/AC were observed due to the presence of mesoporous structure, uniform dispersion, and enhanced interaction between the support and CuSnOS.

2.7 Application of Oxysulfides

In addition to waste water treatment, oxysulfide materials have been utilized in various applications such as hydrogen production, sensor, CO_2 reduction, supercapacitor, etc.

2.7.1 Hydrogen Production

The environmental risks of burning fossil fuels and the ever-growing global demand for energy have inspired researchers to develop renewable and carbon-free energy sources (Tran et al., 2012). Recently, considerable efforts have been given to utilize alternative energy sources such as solar photovoltaic cells, supercapacitors, fuel cells, and batteries. Hydrogen, an ecofriendly fuel with a large specific enthalpy of combustion and clean combustion products, has received a lot of attention as a potential replacement for fossil fuels for dealing with the current energy crisis and pollution (Seger et al., 2012; Yuan, Chen, Yu, & Zou, 2018). Hydrogen can be used to power cars in the same way that other fossil fuels are, or it can be utilized to generate energy using a fuel cell (Yuan et al., 2018). Hydrogen production via photocatalytic water splitting is a very important technique, because it uses renewable feedstock, a green process, and operates in an ambient environment without using pressure or heat (Gholipour, Dinh, Béland, & Do, 2015). Photocatalytic water splitting has been intensively studied since its development by Fujishima and Honda (Fujishima & Honda, 1972).

Catalysts based on TiO_2 and ZnO were widely studied for hydrogen evolution reactions (Do et al., 2020; Lu et al., 2012). Transition metal oxysulfides are a very active catalyst for hydrogen evolution reaction due to their uneven electronic charge distribution across the lattice. In addition, they are more covalent than metal oxide and do not easily oxidize (Sarma et al., 2020). Noble metal-free zinc oxysulfide (Zn(O,S)) nanoparticles were also synthesized by a low-cost chemical reaction at a low process temperature of 70-90 °C for hydrogen evolution reaction with a rate of 3405 µmol/g h (Abdullah, Kuo, & Chen, 2017). Ni-doped Zn(OS) was also reported to enhance the photocatalytic hydrogen evolution of Zn(O,S). A hydrogen production rate of 14,800 µmol/g h was achieved with this catalyst (Gultom, Abdullah, & Kuo, 2017). Co-doped zinc oxysulfide Zn(O,S) solid solution with various concentrations of Co (0-10%) was utilized for the production of hydrogen. The result showed that 2.5% Co-doped Zn(O,S) has the largest amount of photo-evolved hydrogen (H_2) of 27,000 and 1,565 µmol/g under low-power UV light or solar light irradiation respectively (Shuwanto, Gultom, Abdullah, & Kuo, 2020). Different kinds of oxysulfide such as activated

carbon supported AgMoOS (Abdeta et al., 2022), Zi-Ce-Ga oxysulfide (Sisay et al., 2021), WO_xS_y (Sarma et al., 2020), Dy-doped Zn(O,S) (Abdullah, Kuo, & Gultom, 2019), Mo(S,O)/Co(O,S) (Q. Wu et al., 2022), Ag2O/Zn(O,S) (Gultom, Abdullah, Kuo, & Ke, 2019), etc. have been used for hydrogen production application.

2.7.2 Sensor

Recently, due to the development of the internet of things (IoT) different kinds of sensors will be increasingly demanded. Various oxysulfide materials have been used in sensor applications. Neodymium doped lanthanum oxysulfide ($La_2O_2S:Nd^{3+}$) was prepared by the high-temperature solid-state method and reported as an excellent candidate for an optical temperature sensor application (G. Jiang et al., 2014). The result indicated that it could be used in biological applications as well.

Cobalt oxysulfide was also reported as a reversible room temperature hydrogen gas sensor (Zhou et al., 2022). The result showed that excellent performance and a high degree of selectivity over CO_2, NO_2, and CH_4 were observed. Terbium-doped gadolinium oxysulfide ($Gd_2O_2S:Tb$) coated polymethyl methacrylate (PMMA) based optical fiber sensors were also used for monitoring real-time ionizing radiation during radiotherapy (Lewis et al., 2014). The result indicates a distinct and measurable optical signal was obtained when exposed to ionizing radiation due to $Gd_2O_2S:Tb$ scintillation which fluoresces when exposed to ionizing radiation (X-ray). Er-doped lanthanum oxysulfide ($La_2O_2S:Er^{3+}$) powders were also used for temperature sensing applications (Balda, Hakmeh, Merdrignac-Conanec, Arriandiaga, & Fernandez, 2017). Various kinds of oxysulfide materials and their applications are summarized in Table 2.1.

Table 2.1. Oxysulfide materials and their applications

Oxysulfides	**Their application**	**Reference**
Tungsten oxysulfide	NH_3 sensor	(Y. Zheng et al., 2020)
La_2O_2S: Eu^{3+}	Non-contact optical temperature sensor	(G. Jiang et al., 2015)
Janus indium oxysulfide	Chemical sensing	(Xu et al., 2021)
$LiNiS_yO_{2-y}$	Lithium secondary batteries	(Park et al., 2002)
Li_2S-Si-Li_3MO_3 (M=B, Al, Ga, and In) oxysulfide glasses	Lithium secondary batteries	(Hayashi, Komiya, Tatsumisago, & Minami, 2002)
Molybdenum oxysulfide films	Cathodes in lithium and lithium-ion batteries	(Yufit, Nathan, Golodnitsky, & Peled, 2003)
LiAlSO oxysulfide	Lithium superionic conductor	(X. Wang, Xiao, Li, & Chen, 2017)
Zinc oxysulfide	Anode in Li-ion batteries	(Sinha et al., 2018)
Lithium iron Oxysulfides	For Battery Cathodes	(B. Zhu & Scanlon, 2022)
V_2O_4S	Lithium batteries	(Tchangbedji, Odink, & Ouvrard, 1993)
Vanadium oxysulfide	Cathode material for lithium batteries	(Ouvrard, Tchangbédji, Deniard, & Prouzet, 1995)
Lithium titanium oxysulfide	Cathode material for lithium-ion batteries	(Dubois, Pecquenard, Soulé, Martinez, & Le Cras, 2017)
(Cu, M)(O,S) oxysulfide M=Ni, Sn, and Co	Conversion of CO_2 to ethanol	(Xiaoyun Chen, Abdullah, Kuo, Huang, & Fang, 2017)
BiOS	Photocatalytic conversion of CO_2 to CH_4	(L. Jiang et al., 2021)
Cobalt nickel oxysulfide (CoNi) OxSy	High-performance electrode material for supercapacitors	(L. Liu, 2013)

Iron-vanadium oxysulfide (Fe-VOS)	Electrode materials for supercapacitor applications	(Asen, Shahrokhian, & Zad, 2018)
Carbon-cobalt oxysulfide	Electrode for efficient hybrid supercapacitors	(Ranjith et al., 2021)
Manganese-cobalt oxysulfide	Faradaic electrode for charge storage	(M. Liu et al., 2016)
Co-Ni oxysulfide	Electrochemical cells	(Ramulu, Arbaz, & Yu, 2022)
Zn-Co oxysulfide	Faradaic electrode for energy storage.	(Kuai et al., 2017)
$Y_2Ti_2O_5S_2$	Hydrogen production.	(Q. Wang et al., 2019)

2.7.3 Treatment of Organic Pollutants

Various organic pollutants, such as effluent dyes, aromatic compounds (phenol, chloro-phenol, nitro-phenol, and their derivatives), and chlorinated organic compounds (COC), etc. are mainly inter into water bodies from different kinds of sources and pathways, such as industrial wastes, underground household storage, livestock wastes, and hospital sewages (Rojas & Horcajada, 2020). Once these pollutants accumulated in the environment they adversely affect humans and the ecosystem over a long period due to their persistent and hazardous properties. Therefore, effective and efficient removal of organic contaminants is mandatory.

2.7.3.1 Dye Degradation

Different oxysulfide-based catalysts have been used to treat dye-containing wastewater. The CuBiOS oxysulfide catalyst was synthesized to degrade organic dyes (methylene orange, rhodamine B, methylene B) under a dark condition in the presence of $NaBH_4$ (Guo et al., 2020). The CuBiOS catalyst prepared with 0.3 mL of N_2H_4 had reduced above 99% of MO and RhB within 3 minutes and MB within 2 minutes.

Bimetallic In-$Mo(OS)_2$ oxysulfide catalyst was successfully prepared for photocatalytic degradation of RhB, MO, MB, and NR dyes under visible light irradiation. The catalyst was synthesized by a simple precipitation technique at 90 °C by varying the In precursor content to investigate the photocatalytic performance. A 20 mg In-$Mo(OS)_2$ oxysulfide with 20% of

In to Mo precursor molar percentage showed superior catalytic performance and degraded 99.4% RhB (10 ppm), 98.3% MO (10 ppm), 99.6% MB (20 ppm), and 98.4% NR (20 ppm) within 90 min, 180 min, 45 min, and 60 min, respectively. The addition of In to $Mo(O, S)_2$ catalyst created more oxygen vacancy and less adsorbed hydroxyl oxygen which results in the enhancement of photocatalytic activity (Kebede, Kuo, Bekena, & Duresa, 2020).

Heterostructured $Bi_2(O,S)_3/Mo(O,S)_2$ nanocomposite catalyst is also synthesized by a precipitation technique for organic dye remediation under visible light irradiation. It was found that the synthesized $Bi_2(O,S)_3/Mo(O,S)_2$ nano-catalyst enhanced photocatalytic activity, due to well separation and transportation of the charge carriers under photocatalysis than BiOS and MoOS alone. A 96.0% of MO, 96.6% of RhB, 98.8% of MB, and 91.3% of NR dyes were degraded within 180 min, 40 min, 20 min, and 25 min under visible light irradiation, respectively (Bekena, Kuo, & Kebede, 2020).

Photodegradation of methylene blue (MB) was achieved by using a V-doped $Mo(O,S)_2$ catalyst under visible light irradiation. The degradation efficiency of 77.7% was found by using $Mo(O,S)_2$ catalyst, whereas this efficiency is improved by the addition of different molar ratios of Vanadium. The highest degradation efficiency (99%) of MB was obtained using 10% Vanadium doped $Mo(O,S)_2$ catalyst under visible irradiation for 120 min. The results showed that the enhancement of photocatalytic activity is due to the optimal bandgap, the low recombination rate of electron-hole pair, and the low charge transfer resistance (Tadesse, Kuo, Kebede, & Duresa, 2020b).

In addition, the degradation of methyl orange (MO) was studied by using zinc oxysulfide (ZnOS) nanoparticles. Photocatalysis using sunlight require the catalyst to fulfilling the appropriate band gap (2.4 eV to 3.0 eV) for efficient absorption of sunlight for degradation and water splitting. The result reviled that, among the prepared zinc oxysulfide catalyst, $ZnO_{0.6}S_{0.4}$ with a bandgap of 2.7 eV is applicable for degradation of MO in the presence of oxidizing agent H_2O_2 (Pandey, Pandey, Pandey, & Mehrotra, 2013). Kim C. et al. (Kim, Doh, Lee, Lee, & Kim, 2007) also studied the visible light absorptivity of zinc oxysulfide ZnO_xS_{1-x} composite semiconductor and its photocatalytic degradation over organic dyes such as Basic Red 2 (BR2) and 4-chlorocatchol (4-CC). Zincoxysulfide ZnO_xS_{1-x} photo-catalyst prepared by co-precipitation process was a solid solution of both ZnS and ZnO. In zinc oxysulfide, Zn has formed a chemical bonding with both sulfur and oxygen and the bonding was different from that in both ZnS and ZnO. It was obtained that the bandgap energy of ZnO_xS_{1-x} (2.4 eV) is lower than both ZnS (3.5 eV) and ZnO (3.1eV) due to the

formation of hybrid orbitals in the valance band. Therefore, this oxysulfide has superior visible light absorptivity and has become an active component for visible light response. The ZnO_xS_{1-x} showed enhanced photo-degradation performance for the degradation of organic dyes under visible light irradiation.

A bimetallic CuNiOS oxysulfide was synthesized to degrade MB in the dark (Xiaoyun Chen, Kuo, Saragih, et al., 2019). The catalyst is prepared with a different molar ratio of nickel and copper (n(Ni):n(Cu)), and different content of hydrazine (N_2H_4). It was observed that CuNiOS has higher catalytic activity in comparison with CuOS. The complete degradation of MB (10ppm, 100mL) was achieved by using 25 mg CuNiOS with nickel to copper ratio of 3/3 and N_2H_4 of 0% within 5 minutes, whereas, 9.9% MB was degraded within 30 minutes using N_2H_4 free CuOS. In this study, it was found that CuNiOS with a lower Cu^+/Cu^{2+} ratio had a lower oxidation activity (with electrical hole transport between Cu^+ and Cu^{2+}) and with a higher Cu^+/Cu^{2+} ratio had a higher reduction activity (with electron transport between Cu^+ and Cu^{2+}). The reaction trend is shown in Figure 2.3.

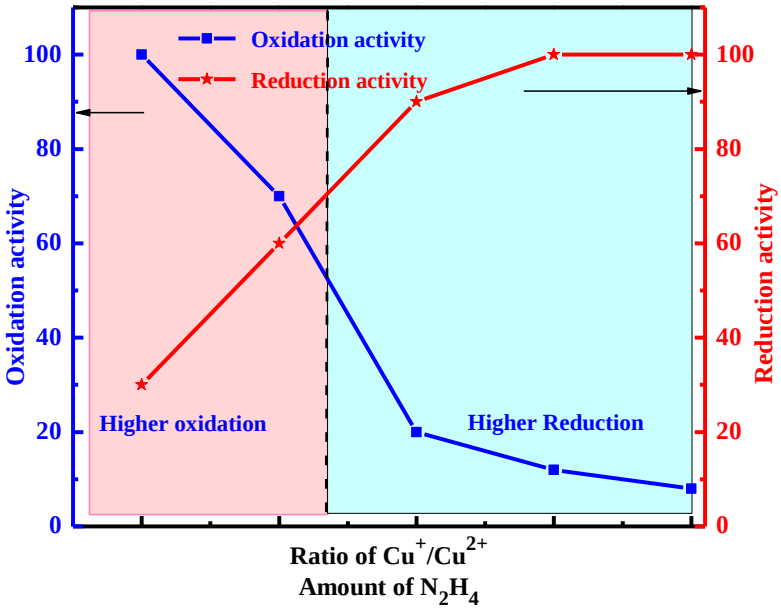

Figure 2.3. The redox reactions catalyzed by CuNiOS in terms of the Cu^+/Cu^{2+} ratio or the N_2H_4 content (Xiaoyun Chen, Kuo, Saragih, et al., 2019).

The photocatalytic degradation of 99.7% MB dye was also obtained within 60 minutes under visible light irradiation by using Sb-doped $Mo(O,S)_3$ oxysulfide nano-plate catalyst (Kebede, Kuo, Zeleke, & Ahmed, 2019). The Sb doping in the molybdenum lattice structure showed a well-crystallized structure with more active species and decreased bandgap energy.

As shown in Figure 2.4, when visible light is applied to the catalyst, electron, and hole pairs were generated but it was found that photo-generated holes were the more responsible active species causing redox reaction with H_2O_2 and H_2O to produce hydroxide radical ($^{\cdot}OH$) that degraded MB dye. The main steps in the reaction mechanism of Sb-doped $Mo(O,S)_3$ oxysulfide photocatalyst were described in Eqn. (1) – Eqn. (4).

$Sb\text{-}Mo(O,S)_3 + hv \rightarrow h^+ + e^-$ ……..Eqn. (1)

$H_2O + h^+ \rightarrow {\bullet}OH + H^+$ .....Eqn. (2)

$H_2O_2 + e^- \rightarrow {\bullet}OH + OH^-$ …….……Eqn. (3)

$h^+ + {\bullet}OH \rightarrow MB \rightarrow$ degradation product ……...Eqn. (4)

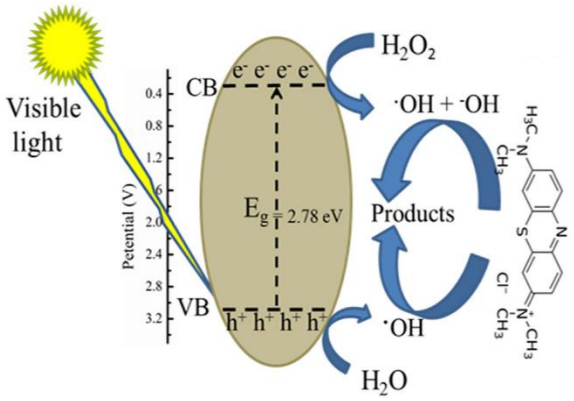

Figure 2.4. The photocatalytic mechanism for degradation of MB dye (Kebede et al., 2019).

The CuNiOS catalyst was synthesized to degrade a highly toxic and low degradable aniline by peroxydisulfate (PDS) (Junyi Zhu, Chen, Li, Zhou, & Lan, 2019). The results indicated that CuNiOS degraded around 80% of the total organic carbon of aniline solution within 20 min. The heterogeneous NiOS catalyst was also prepared and degraded less than 17% of aniline. The degradation performance of CuNiO and CuOS was studied, indicating 27% and 45% reduction, respectively, as compared to CuNiOS. In the degradation process, PDS was critically activated by the copper and nickel ions on the surface of the catalyst.

2.7.3.2 Degradation of Phenol and its Derivatives

Pigments, explosives, plastics, pesticides, and fungicidal agents manufacturing industries discharge hazardous nitro-aromatic compounds to the environment (B. Singh, Kaur, & Singh, 2012). From those nitro-aromatic compounds, 4-nitrophenol and its derivative caused serious effects on humans and the environment. A bimetallic CuVOS oxysulfide was prepared by a facile method with varying N_2H_4 amounts to remove and reduce organic compounds such as 4-NP (H. Sun et al., 2019b). In this study, 5 mg of CuVOS prepared with 0.4 mL of hydrazine completely degraded a 100 mL 4-NP solution in the presence of $NaBH_4$ within 2 minutes. The optimum amount of N_2H_4 changed the surface defect state of CuVOS and resulted in the appropriate amount of n[Cu (I)/Cu(II)] molar ratio to facilitate catalytic acceleration. The stability and reusability of the catalyst were also examined and the result indicated that it can be used repeatedly with excellent reduction performance. The reaction mechanism of 4-NP is shown in Figure 2.5. In step 1, $NaBH_4$ dissociation is occurred and released BH^- which sticks to the catalyst surface. Then, covalent bonding of the hydride ion (step 2) and adsorption of 4-NP on the catalyst surface (step 3) will occur simultaneously. After that, the reaction takes place between the hydride ion and adsorbed nitro group of 4-NP which leads to 4-AP product desorption through electron transfer from BH^{4-} to 4-NP. In addition, V (IV), Cu (I), and Cu (II) will transfer electrons in the reaction.

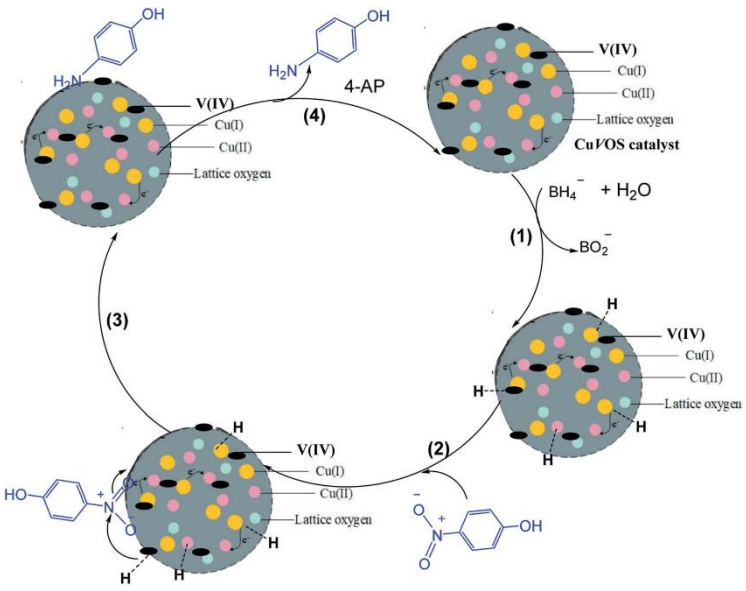

Figure 2.5. The schematic reaction of 4-NP in presence of the CuVOS catalyst (H. Sun et al., 2019b).

Similarly, a CuNiOS and CuOS oxysulfide catalyst was synthesized to study the catalytic degradation of 4-NP and organic compounds. A 10 mg CuNiOS catalyst with Cu to Ni ratio of 1:0.6, completely degraded 4-NP (100 mL, 20ppm) with addition of $NaBH_4$ (0.1M, 3mL) solution within 90 minutes. Whereas, the CuOS catalyst showed lower catalytic efficiency. The results indicated the incorporation of the optimum amount of Ni improved the performance due to the synergetic effect between copper and nickel (Abay, Chen, et al., 2017).

Sn (II)-doped Zn(O,S) oxysulfide was synthesized to reduce 4-nitrophenol (4-NP) to 4-aminophenol (4-AP) by using a hydrogen-evolution assisted photocatalytic reaction (Abdullah & Kuo, 2019). 4-NP was completely reduced to 4-AP within 3 hours without using $NaBH_4$ as a reducing agent. Pure Zn(O,S) nanoparticle's catalytic activity was also tested, but, it did not show the reduction of 4-NP. Sn (II) doping on Zn(O,S) provided a negative site on the catalyst surface to attract the produced hydrogen ion. Therefore, the experimental results indicated that the reduction of 4-NP in an aqueous solution needed UV-light irradiation, Sn (II) doped Zn(O,S), and ethanol.

Zn(O,S) oxysulfide was also doped with rear earth lanthanum metal to reduce toxic 4-NP to less poisonous 4-AP in a 10% ethanol solution without $NaBH_4$ (Abdullah, Gultom, & Kuo, 2019). In this work, the utilization of $NaBH_4$ was replaced by a hydrogen evolved photocatalyst (HEP) as a source of hydrogen ions. The doping of the La to Zn(O,S) lattice improved the adsorption of hydrogen ions on the catalyst surface and promoted 4-NP reduction. An optimum amount of La incorporated into Zn(O,S) was obtained by doping different content of La. It was found that 10%La doped Zn(O,S) of 225 mg catalyst powder in 450 ml ethanol solution was completely reduced 30ppm 4-NP solution within 2 hours of photoreaction. The 10% La-doped Zn(O,S) showed a low photocarrier recombination rate and great electron transfer property with lower resistance. As well, the presence of the surplus photo-generated electrons on the catalyst surface brought on the uptake of electrons by the adsorbed 4-NP molecule.

Photocatalytic reduction of 4-NP to 4-AP by hydrogen evolving catalyst was also achieved by doping Zn(O,S) nanoparticles with magnesium (Bekena, Abdullah, Kuo, & Zeleke, 2019). Photocatalytic reduction efficiency of Mg-Zn(O,S) catalyst was studied by doping 1%, 2.5%, 5%, and 10% of Mg precursor. Zn(O,S) without Mg precursor, was also prepared for comparison. The best catalyst was Mg-Zn(O,S)-2.5 with 2.5% of Mg precursor which reduced 96.7% of 4-NP within 45 minutes, whereas the pure Zn(O,S) reduced only 67.5%

of 4-NP. Doping of Zn(O,S) with more than 2.5% Mg precursor concentration reduced the photocatalytic activity of the catalyst. Because, an excess amount of Mg^{2+} ion concentration will become a recombination center for electron-hole pairs and reduce the active sites on the surface of the Zn(O,S) catalyst that is used for contacting and adsorbing pollutants. The higher content of dopant could notably screen light that reaches the surface of Zn(O,S), leading to lower photocatalytic activity. In this work, hole scavengers called ethanol, Na_2SO_3 formic acid, and EDTA were tested for reduction of 4-NP to 4-AP. The obtained result showed that Na_2SO_3 was the most effective scavenger that consumes photo-generated holes to inhibit its recombination with electrons. Holmium metal was also incorporated into Zn(O, S) lattice to improve the hydrogenation reaction in the conversion of 4-NP into 4-AP (Abdullah, Gultom, Shuwanto, Kebede, & Kuo, 2020). Doping of holmium with an oxidation number of 3^+ (Ho^{3+}) occupies the Zn^{2+} site on a lattice structure and generates a positive charge on the lattice that attracts the photo-generated electron on the catalyst's surface and enhances photo-carrier separation. The negatively charged nitrophenolate ions in the solution of 4-NP were also tested to be attracted to the positively charged Ho atoms on the Zn site for further photocatalytic hydrogenation reaction. It was showed that holmium doping in Zn(O,S) played a great role in reducing nitrophenolate ions diffusion time to the catalyst surface, enhancing the charge transfer, and separating photo-carriers. Therefore, Ho-doped Zn(O, S) catalyst effectively enhanced the hydrogenation reaction to reduce toxic 4-NP to 4-AP with self-generated hydrogen.

2.7.4 Treatment of Inorganic Pollutants

Inorganic chemicals that contaminate water bodies are caused by various reasons. It may occur from drinking water distribution system: Aluminum, copper, iron, lead, zinc, naturally existing substances; fluoride, arsenic, boron, and industrial wastes; heavy metal like mercury, cadmium, chromium, cyanide, etc. (Wasewar, Singh, & Kansal, 2020) Therefore, careful remediation and removal of the contaminants are essential.

2.7.4.1 Arsenic Removal

Arsenic is one of the toxic and carcinogenic inorganic contaminants that pollute water bodies and affect humans and the environment (Sanyal, Bhattacharjee, Paul, & Bhattacharjee, 2020). Natural weathering processes, agricultural and biological activities, volcanic eruption, geochemical reactions, population expansion, mining industry, leaching of

manmade Arsenic compounds, etc., are the factors that result in As pollution of water (Smedley & Kinniburgh, 2001).

Arsenic (As (III and V)) was adsorbed from water using ZnO_xS_{1-x} nanomaterials prepared by wet–chemical route technique. The 2 mg/g concentration of As was efficiently removed from the water within 60 seconds without causing harm to water quality. In the PH range of 6 to 8, greater than 99% absorption was achieved with an adsorption capacity of 299.4 mg/g (Uppal et al., 2019).

Cu-Y binary oxysulfide was prepared by a chemical precipitation technique to study the adsorption of the toxic and carcinogenic arsenic (As III) and As (V)) present in water, and the effect of PH on the adsorption process (Han et al., 2019). As (V) was adsorbed in the PH range of 3 to 10, while As (III) was completely removed in the PH range of 4 to 7. As (III) adsorption performance was reduced to 66% when PH is lowered to 3. In the case of As (V), performance decrease at PH greater than 7 due to electrostatic repulsions of adsorbent active sites (negatively charged) and As (V) anions. The report showed that $\bullet O^{2-}$ which is activated by dissolution and reaction of O_2 with Cu (I) changes As (III) to As (V). Then, the adsorbed As (V) anion and hydroxyl group reacts together and precipitation happens with Y (III) on the adsorbent surface.

2.7.4.2 Hexavalent Chromium Reduction

Hexavalent chromium Cr (VI) inter into the environment and pollute water mainly through discharge from pigment, electroplating, coating, leather manufacturing, and metal processing industries (S. S. Chen, Huang, & Chen, 2014). Hexavalent chromium is categorized as a group I carcinogen by International Agency for Research on Cancer (Yao et al., 2018). Thus, effective treatment of hexavalent chromium before discharging it into water is a very crucial activity. The reduction of Hexavalent chromium Cr (VI) into less toxic and more stable trivalent chromium Cr (III) plays a great role in chromium treatment.

Hetro-structure $Bi_2(O,S)_3$/Zn(O,S) composite was synthesized by a solvothermal method without any surfactant addition for reduction of Cr (VI) (Ahmed, Kuo, & Kebede, 2019). The $Bi_2(O,S)_3$ and Zn(O,S) were also prepared separately to study their catalytic reduction activity. The 40% of Cr (VI) was reduced by a $Bi_2(O,S)_3$ oxysulfide catalyst, whereas no catalytic reduction was observed with Zn(O,S) catalyst. The composite $Bi_2(O,S)_3$/Zn(O,S) catalyst with a Bi/Zn ratio of 20% reduced 99.5% of Cr (VI) under visible light irradiation

within 12 minutes. The $Bi_2(O,S)_3$/Zn(O,S) composite catalytic activity under dark was also studied and 80% Cr(VI) reduction was achieved. The reaction of Cr (VI) reduction to Cr (III) under visible light is shown in Eqn. (1) and (2):

$CrO_4^{2-} + 4H_2O + 3e \rightarrow Cr(OH)_3 + 5OH^-$ …….. Eqn. (1)

$Cr2O_7^{2-} + 14H^+ + 6e \rightarrow 2Cr^{3+} + 7H_2O$ ……... Eqn. (2)

The reduction mechanism of Cr (VI) is illustrated in Figure 2.6. The formation of the hydroxyl group on the catalyst surface played a great role in increasing catalytic reduction activity. Electron could not exit from the valance band to the conduction band of Zn(O,S) due to its wide bandgap. But in the case of $Bi_2(O,S)_3$ electrons can jump to the conduction band due to its small bandgap. These electrons could also jump to the conduction band of Zn(O,S) and inhibit the electron-hole recombination rate that provides additional electrons for catalytic reduction.

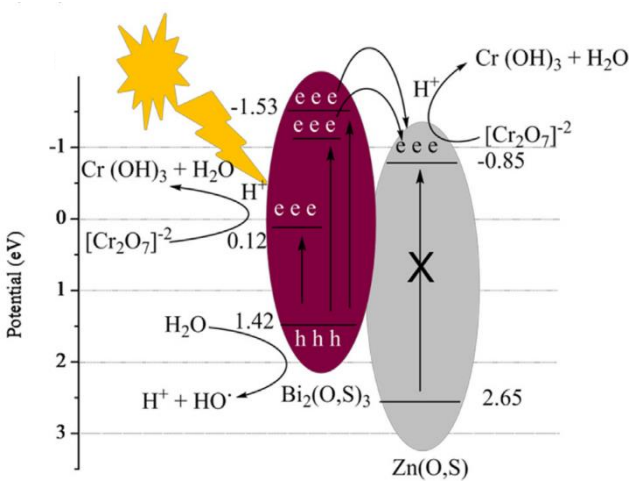

Figure 2.6. The proposed mechanism for $Bi_2(O,S)_3$/Zn(O,S) composite photocatalyst to reduce Cr(VI) (Ahmed et al., 2019).

The $In_2(O,S)_3$ nanosheet was also successfully synthesized to study the catalytic reduction of hexavalent chromium and the evolution reaction of hydrogen. A complete reduction of Cr (VI) was achieved by using $In_2(O,S)_3$ catalyst under visible light irradiation within 15 minutes. $In_2(O,S)_3$ did not show any catalytic reduction under dark conditions. Annealing of $In_2(O,S)_3$ catalyst at different working temperatures was also studied and the results indicated that low annealing at 90 °C for 2 hours showed better photocatalytic performance (Abdullah, Gultom, et al., 2017).

Reduction of Cr (VI) into metallic Cr (0) was reported by using bimetallic CuInOS oxysulfide catalyst under dark (Xiaoyun Chen & Kuo, 2017). A 20 mg CuInOS catalyst was completely reduced 100 ml Cr (VI) of 50 mg/L within 4 min without any reagent and light irradiation. CuOS oxysulfide catalyst was synthesized without the addition of In and only 8% of Cr (VI) was reduced within 10 min. In this report, the reduction efficiency of CuInOS catalyst was also studied by varying catalyst amounts. As the catalyst content was increased, catalytic activity and reduction performance were also improved well. Catalytic reusability and stability were investigated and a reduction of 91.8% was achieved after using CuInOS for six-run. The catalyst had a good reduction performance in the PH range of 4-7. In the process, Cr (VI) was reduced to intermediary Cr^{3+} and finally to metallic Cr (0). Faster Cr(VI) reduction in the dark was related to Cr (VI) and water due to structural defects, an interfacial reaction within the catalyst, and reduced amount of Cu^{+} and S^{6+} which distort the lattice, weaken the lattice bonding, and form anion vacancy.

The (Sn, Zn)(O,S) oxysulfide nano-catalysts were synthesized by varying amounts of Zn to investigate the reduction of hexavalent chromium Cr (VI) to Cr (III) under visible light (Zelekew et al., 2019). A complete reduction of hexavalent chromium was obtained by using (Sn, Zn)(O,S) catalyst with Sn: Zn molar ratio of 80:20 within 80 min. Sn(O,S) catalyst prepared without the addition of any Zn content were reduced 85.6% Cr^{+6}. The synergetic effect between Sn and Zn and the optimum amount of Zn improved the catalytic efficiency of the catalyst.

In addition to hexavalent chromium Cr(VI), heavy metal reduction such as Pb (II) and Mg (II) as well as the organic dye was investigated by using tubular bimetal CuMgOS oxysulfide catalyst under dark (Xiaoyun Chen, Kuo, Zhang, Lu, Lin, et al., 2019). The 20 mg CuMgOS catalyst synthesized with 0.3ml hydrazine was completely reduced 100 ml Cr (VI), Pb(II), and Hg(II) of 50 ppm within 4 min, 6 min, and 4 min respectively, but, a 49.3% reduction was obtained with CuMgOS-0 in 5min. A good catalytic activity under the dark condition without any other reagent addition was obtained by using the appropriate amount of hydrazine to optimize the n[Cu(I)/Cu(II)] ratio for enhanced Cr (VI) reduction.

Bimetallic $(In,Ga)_2(O,S)_3$ oxysulfide catalyst was synthesized with different Ga contents with a facile method at a temperature of 150 °C for photocatalytic reduction of hexavalent chromium (Cr(IV)) (Zeleke, Kuo, Ahmed, & Gultom, 2018). The result indicated that photocatalytic reduction activity is improved and electrical property is increased with the incorporation of Ga as compared to pure $In_2(O,S)_3$ oxysulfide catalyst. The $(In,Ga)_2(O,S)_3$

oxysulfide catalyst was completely reduced Cr (IV) to Cr (III) under visible light irradiation within 4 minutes. Similarly, a nanocomposite of V_2O_5 and $(In,Ga)_2(O,S)_3$ was prepared and reduced Cr (IV) within 2 minutes under visible light irradiation (Zeleke & Kuo, 2019). The V_2O_5 nanoparticles were finely dispersed and loaded on the surface of $(In,Ga)_2(O,S)_3$ nano-flower catalyst, enhancing the charge carrier's transition between the two phases. The nanocomposite catalyst exhibited an amorphous-like nature, better electrical properties, and substantially improved Cr (IV) reduction capability compared to the pure counterpart catalyst. The rate constant of nanocomposite catalyst (1.73 min^{-1}) was improved by 3.6 fold compared to $(In,Ga)_2(O,S)_3$ oxysulfide catalyst.

Moreover, nano-sheet CuSbOS oxysulfide catalysts were prepared for the reduction of heavy metal ions and organic dyes (Xiaoyun Chen, Kuo, Zhang, Lu, & Lin, 2019). The CuSbOS with the appropriate amount of N_2H_4 exhibited better reduction performance for Cr (VI), Pb (II), and Hg (II) without any other reducing agent and photo energy, and for MO, MB, and RhB with the addition of $NaBH_4$. The effect of PH on the catalytic reduction of Cr (VI) was tested and CuSbOS showed the highest catalytic activity over a wide PH range of 3-6. Good durability and stability were also observed after testing the catalyst repeatedly for the reduction of both heavy metal ions and organic dyes. The carrier hopping between Cu (I) and Cu (II), and the surface reaction center of bimetallic oxysulfide catalyst that interacts with reactants resulted in excellent catalytic performance. The catalytic activity of some oxysulfide catalysts on the degradation of organic and inorganic pollutants is summarized in Table 2.2.

Table 2.2. Summary of Oxysulfide-based catalysts and their catalytic activity.

Catalysts	**Amount (mg)**	**Type**	**Pollutant (mL)**	**Light type**	**Time (min)**	**Efficiency (%)**	**Ref.**
CuVOS	5	4-NP MO MB RhB	100 100 100 100	Dark	2 2 5 6	100 100 100 100	(H. Sun et al., 2019b)
CuBiOS	5	4-NP MO RhB MB	100 100 100 100	Dark	2 3 3 2	100 >99 >99 >99	(Guo et al., 2020)
$InMo(OS)_2$	20	RhB MO MB NR	100 100 100 100	Visible light	90 180 45 60	99.4 98.3 99.6 98.4	(Kebede et al., 2020)
$VMn(OS)_2$	20	MB	100	Visible light	120	99	(Tadesse et al., 2020b)
LaZn(OS)	225	4-NP	450	UV-light	120	100	(Abdullah, Gultom, et al., 2019)
MgZn(OS)	200	4-NP	400	UV-light	45	96.7	(Bekena et al., 2019)
$Bi_2(O,S)_3$/ Zn(O,S)	20	Cr(VI)	50	UV-light	12	99.5	(Ahmed et al., 2019)
$InGa_2(OS)_3$	0.2g/L	Cr(VI)	100	Visible light	4	100	(Zeleke et al., 2018)

Among various reported waste water treatment techniques, catalytic reduction reaction received great interest due to its simplicity, high efficiency, low cost, a useful byproduct, quick process, and complete removal of dyes. Noble metal catalysts such as Rh, Ru, Pd, Pt, and Au nanoparticles have been widely used for the catalytic reduction of organic dyes in

the presence of sodium borohydride due to their excellent catalytic performance (Pradeep, 2009). However, the scarcity of noble metals and their high cost severely limit the catalytic application of noble metal nanoparticle-based catalysts (Tian, Dong, Cui, & Dong, 2016). Researchers are currently working to develop new types of non-noble metal catalysts with superior catalytic performance to replace noble metal nanoparticle catalysts. The transition metal catalysts such as nickel (Ni), cobalt (Co), iron (Fe), copper (Co), and manganese (Mn) have attracted great interest in catalysis application due to high abundance, low cost and excellent thermal stabilities (Xiaoyun Chen, Kuo, Wu, et al., 2019; Dube, Moutloali, & Malinga, 2020; Ravindhranath & Ramamoorty, 2017; Shu, Lan, Gao, Wang, & Huang, 2015). Among them, nickel-based catalysts such as nickel oxide, nickel hydroxide, and nickel sulfide have attracted enormous attention due to their low cost, non-toxicity, and high chemical stability (Ran et al., 2012; Zelekew & Kuo, 2017b). They are utilized in a wide range of applications such as magnetic materials, electrochemical supercapacitors, fuel cell electrodes, electrochemical films, rechargeable batteries, and catalysis for water purification due to their promising chemical and physical properties (Cheng, Le, Cai, & Yu, 2011; Ran et al., 2012). Chen X. et al. (Xiaoyun Chen, Kuo, Saragih, et al., 2019) Synthesized bimetallic CuNiOS oxysulfide catalyst for degradation of MB under dark. They studied the effect of Cu^{+}/Cu^{2+} ratio and incorporation of Ni on redox reaction. It was found that CuOS (without Ni) did not show any redox reaction at all because it can form strong bonding with anions since there are no extrinsic cations of Ni to distort the lattice. Thus, it is difficult to transport the hopping charge for redox reaction since it becomes localized. Degradation of 4-nitrophenol (4-NP) and rhodamine-B (RhB) (Abay, Chen, et al., 2017), and aniline (Junyi Zhu et al., 2019) using CuNiOS oxysulfide catalyst was also reported. Ethiraj A.S et al. (Ethiraj, Uttam, Varunkumar, Chong, & Ali, 2020) prepared Cu-doped nickel oxide nanoparticles to degrade 4-nitro phenol under UV irradiation. The results indicated that the Cu-NiO nanocatalyst exhibited a good phenol degradation performance than its undoped counterpart. Akbari A. et al. (Akbari et al., 2020) studied the effect of NiO nanoparticles as a photocatalyst and suggested that the use of NiO for photocatalytic removal of a cationic dye such as MB can be a suitable approach.

Manganese-based compounds (mainly oxides) are low-cost, high abundance transition metals and exhibited excellent electrochemical performance due to their high theoretical capacity, high redox activity of metal ions, and eco-friendliness (M. Liu et al., 2016; Y. Zhang et al., 2018; Jian Zhu, Tang, Xie, Dai, & Meng, 2014). Liu M. et al. (M. Liu et al.,

2016) prepared flower-like manganese-cobalt oxysulfide supported on Ni foam as a faradaic electrode to store charge. The results showed that manganese cobalt oxysulfide could be a promising electrode for energy storage device applications. Li W. et al. (W. Li et al., 2021) synthesized a nano-scale catalyst consisting of copper-manganese bimetallic oxysulfide for degradation of 2,4,6 trichlorophenol.

As reported in the above literature review, oxysulfide materials are synthesized by using a strong reducing agent, hydrazine hydrate (N_2H_4). Hydrazine is an extremely toxic, poisonous, and carcinogenic chemical (Bollard et al., 2005; Mohammad, Khan, & Cho, 2020). Excessive hydrazine inhalation can cause damage to the lung, liver, kidney, and central nervous system (Kaur, Raza, & Branda, 2021). It adversely affects human health and corresponding process at least in two ways. One of these is the formation of hydrazone derivatives by reacting hydrazine with α-keto acids of cellular active molecules (e.g., vitamin B6 derivatives) which hinders essential life activities such as amino acid decarboxylation and transamination, nucleic acid and lipid metabolism, and mitochondrial oxidation (X.-Y. Zhang, Yang, Wang, Jiao, & Zhu, 2020). The other way involves the formation of intermediate free radicals, such as methyl, acetyl, hydroxyl, and hydrogen radicals, which damage protein, mitochondrial DNA, and other macromolecules as well as chromosomal DNA (J. Wang et al., 2018; X.-Y. Zhang et al., 2020). Therefore, we are interested in designing oxysulfide catalyst that is environmentally friendly and non-toxic to human health.

In this work, we synthesized a novel flower-like bimetal NiMnOS oxysulfide catalyst with an ecofriendly, simple, and facile preparation technique at the low temperature of 90 °C for the reduction of organic dyes in an aqueous solution. The oxysulfide NiMnOS catalysts were characterized by XRD, XPS, SEM/EDS, FTIR, and UV-Vis spectroscopy. The catalytic activity of the as-synthesized catalysts was evaluated by the reduction of methylene blue dye with $NaBH_4$. The possible reduction mechanism with NiMnOS catalyst was also proposed. Due to the synergistic effects of the two metals, bimetallic NiMnOS systems exhibited high catalytic efficiency.

CHAPTER THREE

3. Experimental Methods

3.1 Chemicals

The chemicals used in this experiment were Manganese (II) sulfate monohydrate [$MnSO_4.H_2O$, Alpha Chemika, 98%], Nickel acetate tetrahydrate [$Ni(CH_3COO)_2.4H_2O$, Loba Chemie, 98%], Thiourea [CH_4N_2S, Finkem], sodium borohydride [NaBH4, Alpha Chemika, 97%], Methylene blue [SDFCL], and ethanol. Distilled water was used throughout the experiment. These chemicals were commercially available and used without purification.

3.2 Synthesis of NiMnOS Catalyst

The bimetallic NiMnOS samples were prepared as shown in Figure 3.1. In a typical synthesis, 10 mmol of $Ni(CH_3COO)_2.4H_2O$ was dispersed in 400 mL of distilled water under magnetic stirring at room temperature and a light green solution was formed. Then, 30 mmol of $MnSO_4.H_2O$ was added to the solution under vigorous stirring. Subsequently, 40 mmol of H_2NCSNH_2 was added to the above mixture and stirred for 30 min to incorporate sulfur. The aforesaid mixture was transferred into four holes water bath and reacted for 5 hours at 90 °C. After the reaction was completed, the solution was naturally cooled to room temperature and centrifuged to obtain the precipitate. The collected precipitate was washed several times with distilled water and ethanol. Finally, it was dried in an oven at 80 °C for 12 hours. After being dried, the resulting precipitate from Ni: Mn molar ratio of 25:75 was abbreviated as NiMnOS-25. The other samples, with Ni: Mn molar ratios of 50:50 and 75:25 were prepared with the similar procedure described above and denoted as NiMnOS-50, and NiMnOS-75, respectively. For comparison, MnOS and Mn-free NiOS catalysts were prepared using the same approach.

Figure 3.1. The schematic diagram for the synthesis of the NiMnOS catalyst

3.3 Characterization of the Catalyst

The phase purity and crystal structure of the as-synthesized samples were measured by X-ray powder diffraction (XRD) (SHIMADZU XRD-7000) with monochromatic Cu Kα radiation (λ=1.5418 Å). The samples were examined in the 2θ range from 10° to 80° at a scanning speed of 3 degrees/minutes using a voltage of 40 kV and filament current of 30 mA. The X-ray photoelectron spectroscopy (XPS) studies were conducted using an ESCALAB photoelectron spectrometer. The surface morphology and elemental analysis of the as-prepared samples were examined by Scanning electron microscopy (SEM) equipped with Energy-dispersive X-ray spectroscopy (EDS) (JSM 6500F, JEOL). Functional group examination was carried out by Fourier transform infrared (FTIR) spectra (Spectrum 65 FT-IR, Perkin Elmer) in the wavenumber range of 400-4000 cm^{-1} using KBr pellets. Ultraviolet-visible (UV-Vis) absorption of the as-prepared samples was studied using UV-Vis Spectroscopy (Shimadzu–3600 Plus). Catalytic reduction of methylene blue was examined by Shimadzu–3600 Plus UV–vis spectrophotometer.

3.4 Catalytic Reduction Activity of the Catalyst

The catalysts were tested for the reduction of Methylene Blue (MB). Specifically, 30 mg of $NaBH_4$ was added into 100 mL (10 ppm) of MB solution under stirring. Then, 30 mg of NiMnOS catalyst was added to the mixture to start the reduction reaction. The methylene blue reduction reaction was carried out at room temperature. The color of the mixture gradually changed from blue to colorless, indicating that the reduction reaction had been completed. The concentration of MB was monitored at the time interval of 2 minutes by using UV–Vis spectrophotometer. The degradation efficiency of the above reaction was calculated according to Beer-Lambert's law (Eqn. (3.1)) (Xia, Liu, Shi, & Zhang, 2019).

$$D\ (\%) = \left(\frac{A_o - A_t}{A_o}\right) \times 100 \quad \ldots\ldots\ldots\ldots\ldots\ldots\ldots\ldots \text{Eqn. (3.1)}$$

Where A_0 represented the initial absorbance of the substrate solution and A_t represented the absorbance of the substrate solution at various time intervals.

The stability and reusability of the NiMnOS-25 catalyst were also tested. Particularly, 150 mg of $NaBH_4$ has been added into 500 mL of MB (10 ppm) aqueous solution. Then, 150 mg of NiMnOS catalyst was added under stirring. The reduction of MB solution was determined by using UV–Vis spectrophotometer. After the first round was completed, the resulting solution was made to settle and the upper layer of the solution was removed. Then, the remaining solution with the catalyst was centrifuged and washed with water and ethanol. Finally, the powder was dried in an oven at 80 °C for 12 hours. The dried powder was utilized in the second run experiment using the same procedure as the first. The third, and fourth run experiments also followed a similar pattern as stated in the first round.

CHAPTER FOUR

4. Result and Discussion

4.1 XRD Analysis

X-ray diffraction was used to assess the overall crystallinity and purity of the produced samples. Figure 4.1 shows the XRD diffraction patterns of the as-synthesized NiOS, NiMnOS-75, NiMnOS-50, NiMnOS-25, and MnOS samples. The bare MnOS (Figure 4.1e) showed poor crystallinity with the main diffraction peaks at 2θ of 32.9, 33.9, 36.02, 43.4, 55.2, 58.6, 60.4, 64.3, and 65.7 correspond to the $MnO_3S_{0.6}$ (JCPDS card no. 00-021-0556). The diffraction peaks observed at 2θ of 29.3, 33.2, 36.1, and 54.7 can be ascribed to the (200), (210), (211), and (023) planes of cubic MnS_2 (JCPDS card no. 01-076-2047). The XRD pattern of NiOS (Figure 4.1a) showed that the main diffraction peaks at 2θ value of 12.14°, 24.44°, 33.28°, 36.94°, 59.4° and 70° corresponds to (0 0 1), (0 0 2), (1 1 0), (1 1 1), (3 0 0) and (2 2 0) planes, respectively, of hexagonal $3Ni(OH)_2.2H_2O$ (JCPDS No.00-022-0444). As we observed, the as-prepared NiOS exhibited a crystalline structure. The diffraction patterns of NiMnOS-75 (Figure 4.1b), NiMnOS-50 (Figure 4.1c), and NiMnOS-25 (Figure 4.1d) indicate a broad peak of $3Ni(OH)_2.2H_2O$ with lower intensity. In addition, the marginal shift of XRD peaks to lower angles was also observed, which shows that the addition of Mn did change the original phase of the material. These peak shifts in the XRD may be due to the change in the crystal lattice which is caused by the incorporation of Mn, a higher ionic radius, into Ni sites. The decrease in diffraction intensity is also indicated that the crystallinity of the material is decreased due to the addition of manganese. In addition, the low synthesis temperature below 100 °C may result in poor crystallization and nanopowder size which is contributed to the weakening and broadening of NiMnOS peaks (Xiaoyun Chen, Kuo, Zhang, Lu, & Lin, 2019). There were no further secondary phases found, indicating that the as-prepared NiMnOS catalyst is a solid solution-type single phase.

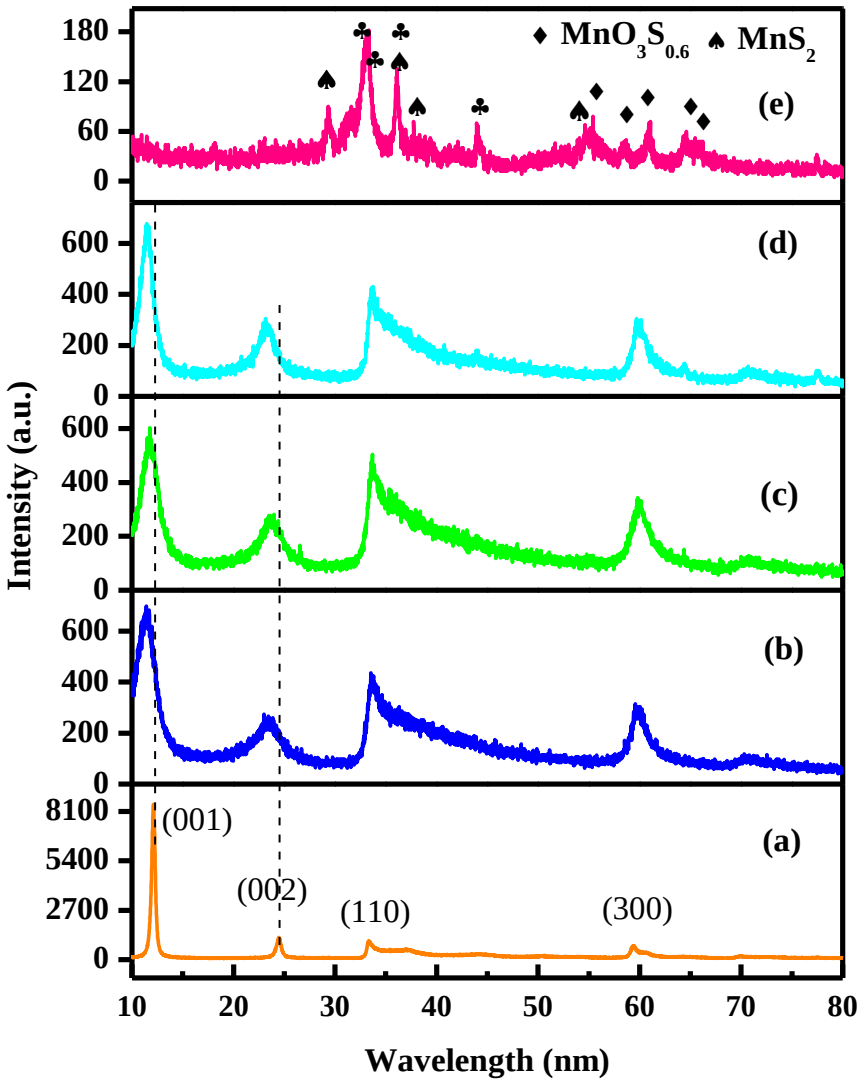

Figure 4.1. X-ray diffraction pattern of (a) NiOS, (b) NiMnOS-75, (c) NiMnOS-50, (d) NiMnOS-25, and (e) MnOS.

The crystallite size of the catalysts was calculated by the Scherrer equation (Eqn. 4.1) (Jafari & Afshar, 2016).

$$D = \frac{0.9\lambda}{\beta cos\theta} \quad \text{..... Eqn. (4.1)}$$

Where D is the crystallite size, λ is the wavelength of the incident X-ray (1.54nm), β is the full width at half maximum of the diffraction peak (FWHM), and θ is the Bragg diffraction angle. The NiMnOS oxysulfide catalysts have a smaller crystallite size than the bare NiOS catalysts produced. The average crystallite size of NiMnOS catalysts was estimated to be in the range of 3.19-3.80 nm, whereas the crystallite size of bare NiOS is around 8.25 nm. The

incorporation of larger manganese can lead to lattice distortion, which in turn is responsible for the change in crystallization and its crystallite size.

4.2 XPS Analysis

The chemical binding and ionization state of the as-synthesized NiMnOS-25 catalyst was investigated using XPS analysis. As shown in Figure 4.2a of Ni spectrum, the two major peaks with binding energies at 872.75 and 855.1 eV, represent the Ni $2p_{1/2}$ and Ni $2p_{3/2}$ levels, respectively. The Ni $2p_{1/2}$ and Ni $2p_{3/2}$ with the energy gap separation of 17.65 eV and the two satellite peaks located at 860.8 and 878.85 eV indicate the existence of Ni^{2+} in NiMnOS-25 (Yue et al., 2018). The Mn 2p XPS spectrum showed that the peak of Mn 2p1/2 and Mn 2p3/2 located around 652.17 and 641.2 eV, respectively, with the separation energy gap of 10.97 eV, indicating the existence of Mn^{3+} ions. The peak position at 644.9 and 654.05 eV ascribed to Mn 2p3/2 and Mn 2p1/2 bands, respectively, corresponds to Mn^{4+} ion (Hui Chen et al., 2018; Xue et al., 2017). The O 1s XPS spectra in the NiMnOS-25 catalyst show (Figure 4.2c) that the peaks at 531 eV and 530 eV corresponds to the hydroxyl oxygen and the lattice oxygen, respectively (H. Sun et al., 2019a). The S 2p XPS spectra of NiMnOS are also displayed in Figure 4.2e. The S 2p peaks at a binding energy of 168.55 eV belong to S^{6+} (Xiaoyun Chen, Sun, Zhang, Guo, & Kuo, 2019) and at 167.2 eV show the S-O bonding with sulfate features (Tang et al., 2017).

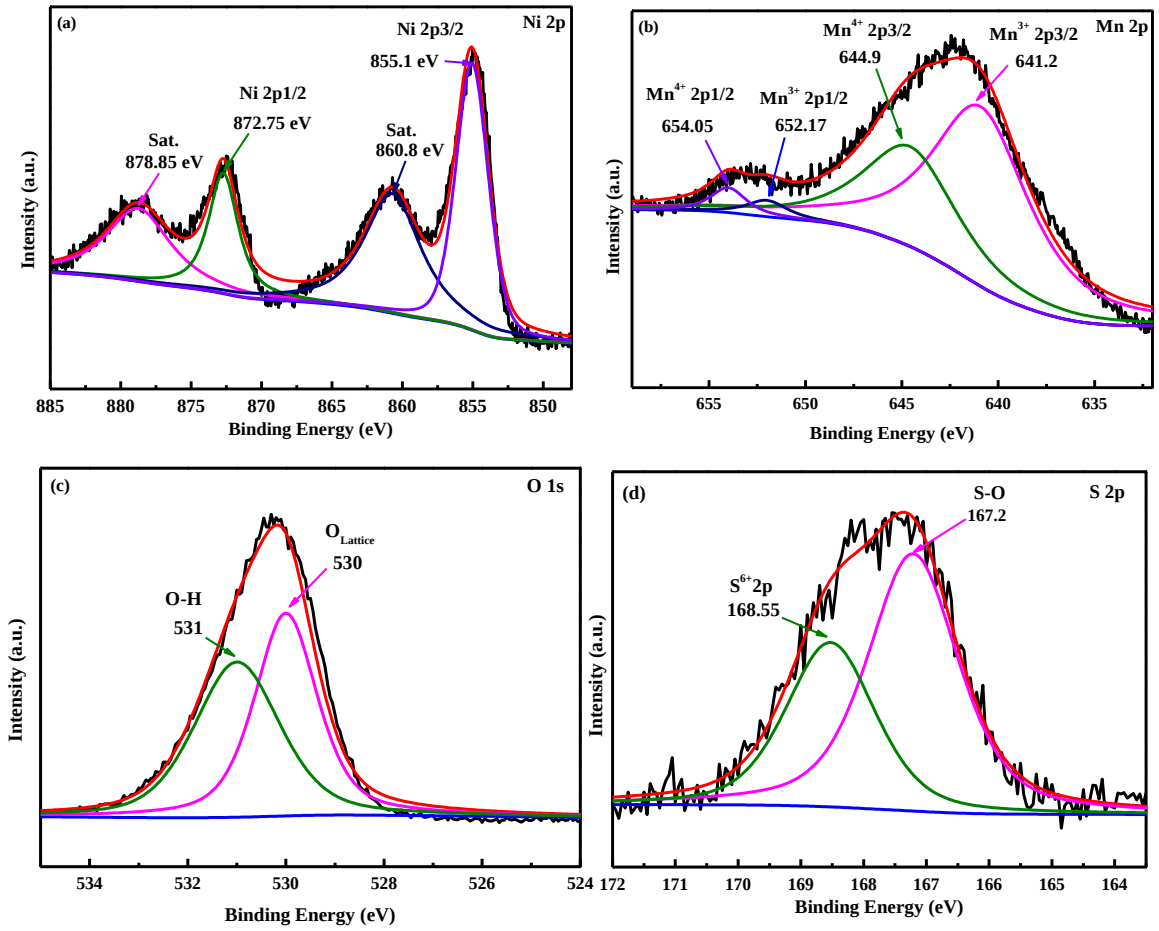

Figure 4.2. XPS spectra of (a) Ni 2P, (b) Mn 2p, (c) O 1s, and (d) S 2p in the NiMnOS-24

4.3 SEM and EDS Analysis

The morphology and structure of the as-synthesized NiOS, MnOS, and NiMnOS-25 catalysts were investigated using Scanning Electron Microscope (SEM). The SEM morphologies of NiOS, MnOS, and NiMnOS-25 catalysts were shown in Figure 4.3a, b, and c. As seen in Figure 4.3a, bare NiOS shows a sheet-like structure with a larger size. The morphology of MnOS is also shown in Figure 4.3b and exhibits aggregated nanoparticles with various sizes ranging from small to big particles size. The variation in particle size is occurred due to the formation of some small particle aggregate. As can be seen from Figure 4.3c, the as-synthesized NiMnOS-25 exhibited a flower-like structure with uniform morphology.

The flower-like shape in the structure has more space and open channels, which provides more interaction sites for reduction reactions to occur. The elemental composition of the as-synthesized catalyst was investigated by using energy-dispersive X-ray spectroscopy (EDS).

Figure 4.3d shows, the elemental analysis of as-prepared NiMnOS-25. The result proves the presence of nickel (Ni), manganese (Mn), oxygen (O), and sulfur (S), and shows the successful synthesis of bimetallic NiMnOS oxysulfide catalysts.

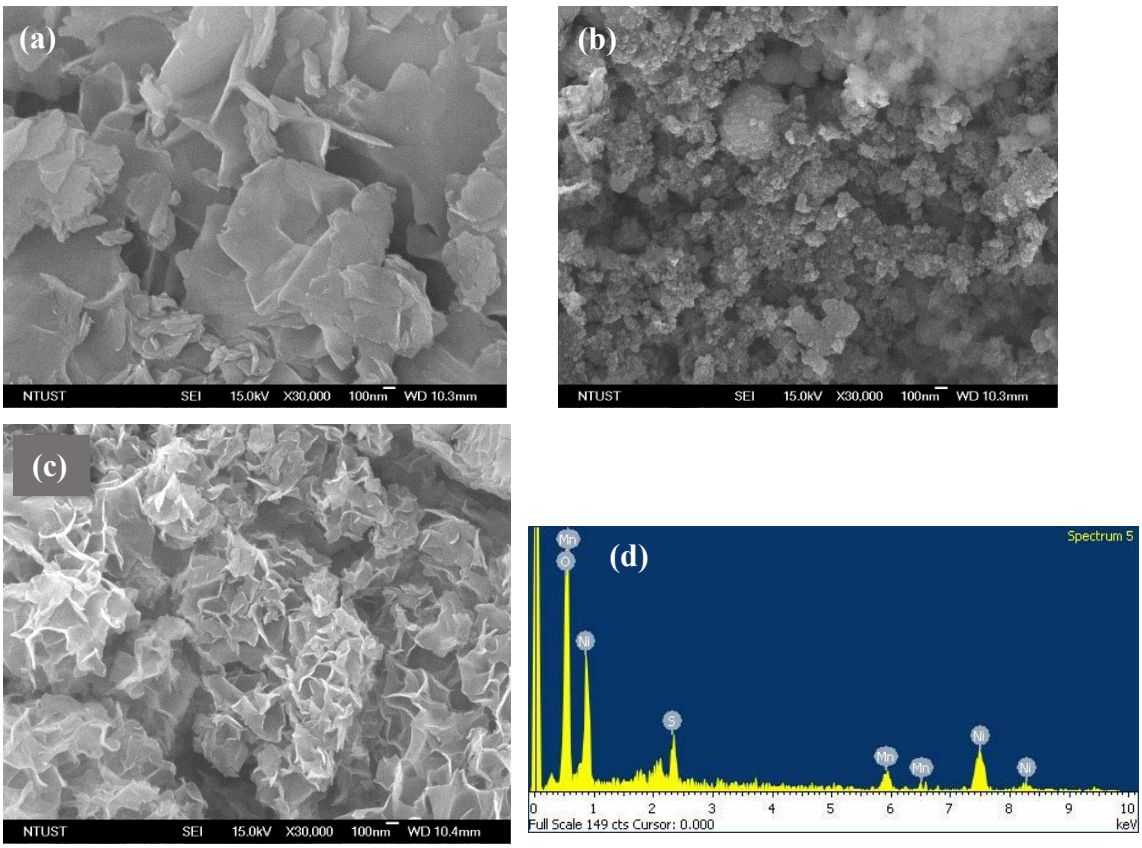

Figure 4.3. SEM images of (a) NiOS, (b) MnOS and (c) NiMnOS-25, and (d) the EDS spectrum of NiMnOS-25 catalyst.

4.4 Optical Property Analysis

The UV–Vis absorption spectra of NiMnOS catalysts produced with various molar percentages of Ni/Mn are shown in Figure 4.4a. It was observed that with increasing the Mn content, the bimetallic NiMnOS oxysulfide had better absorbance of visible light. The samples exhibit a broad wavelength absorption range, indicating that the sample band has more absorption states or defects.

The direct bandgap (Eg) of the samples was calculated from UV–Vis absorption spectra by using the standard Tauc method (Sharrouf, Awad, Roumié, & Marhaba, 2015).

$$(\alpha \mathrm{h}v)^2 = k(\mathrm{hv} - \mathrm{E}g) \ldots\ldots\ldots\ldots\ldots\ldots\ldots\ldots Eqn.\ (4.2)$$

Where α = 2.303 A/L, A is the absorbance of the sample and L is the path length (1 cm), h is the Planck constant, k is the absorption constant for direct transition, hν is the absorption energy, and Eg is the bandgap. Figure 4.4b shows the $(\alpha h\nu)^2$–hν curves of NiMnOS catalysts prepared with different Ni/Mn molar percentages, together with NiOS and MnOS. The band gaps of NiOS, NiMnOS-75, NiMnOS-50, NiMnOS-25, and MnOS were obtained as 3.94, 3.54, 3.28, 2.37, and 2.57 eV, respectively. It is observed that the Eg value of bimetallic NiMnOS decreased when the amount of Mn increased. Compared with the band gap value of NiO at 3.6-4 eV (M. Shi et al., 2021), MnO at 3.6-4.2 eV (Lim, Saldana-Greco, & Rappe, 2016), MnO_2 at 1.3 eV (Cockayne & Li, 2012), NiS at 0.9 eV (Addawiyah & Gunlazuardi, 2018), MnS at 3.1 eV (Chaki, Chauhan, Tailor, & Deshpande, 2017), the variation of bandgap energy values show that NiMnOS is a bimetal oxysulfide in the form solid solution (Xiaoyun Chen, Kuo, Zhang, Lu, & Lin, 2019).

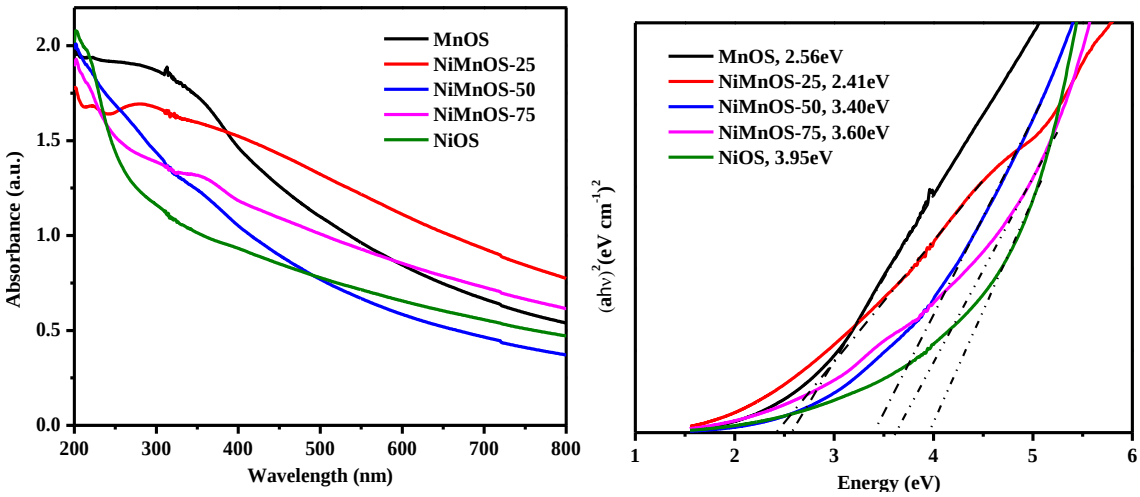

Figure 4.4. (a) UV–Vis absorption spectra, (b) the $(\alpha h\nu)^2$-hν plot from the UV–Vis absorption

4.5 FTIR Analysis

Fourier transform infrared (FT-IR) studies were conducted in the range of 4000-400 cm^{-1} to identify the functional groups of the as-prepared samples as shown in Figure 4.5. The broad peak in the range of 3000–3700 cm^{-1} relates to the O–H stretching vibrations of non-hydrogen bonded O-H, hydrogen-bonded hydroxyl groups, and the interlayer water molecules in the structure (Z. Zhang et al., 2021). The broadening of the band is due to the formation of hydrogen bonds (Taibi et al., 2002). The band at 1630 cm^{-1} was ascribed to the

bending vibration mode of interlayer water molecules (H.-Y. Wu, Xie, & Hu, 2013). The band around 1012 cm^{-1}, in Figure 4.5a, is occurred due to the stretching vibration of C-O bond (Baruah, Kalita, & Narayan, 2019; Jansi Rani et al., 2019). As shown in Figure 4.5c, the intense band at 1068 cm^{-1} displayed the presence of S-O bond due to the SO_3^- group from Mn source precursor (Oriakhi, Farr, & Lerner, 1996; Poul, Jouini, & Fiévet, 2000).

In Figure 4.5b the peak shift to the higher wavenumber is observed in the case of NiMnOS-25, which implies the incorporation of Mn. In addition, both C-O and S-O bonds were observed at 1038 cm^{-1} and 1112 cm^{-1}, respectively. The band around 638 cm^{-1} is associated to the bending mode of M-O bond (M=Mn, Ni), and the band below 500 cm-1 can be due to the stretching vibration of M-O bond (Dong et al., 2019; J. Li, Wei, Chu, & Wang, 2017).

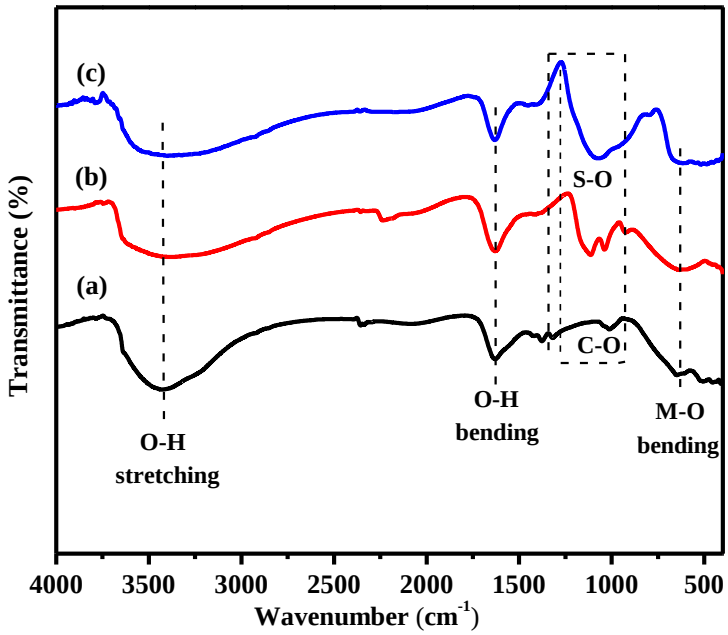

Figure 4.5. FT-IR spectra of (a) NiOS, (b) NiMnOS-25 and (c) MnOS

4.6 Catalytic Reduction of Methylene Blue

The performance of the catalyst was assessed with the reduction of MB in an aqueous solution. Figure 4.6 indicates the catalytic performance of the NiMnOS catalysts towards the reduction of MB to Leuco-methylene blue (LMB) in the presence of $NaBH_4$. MB is a heterocyclic aromatic dye that is water-soluble and mostly exist in an ionic (MB^+) form in an aqueous solution (Abay, Chen, et al., 2017). UV-vis absorption peaks of the oxidized form of MB exist in the wavelength (λ) range of 550-750 nm, with an absorption maxima at λmax = 664 nm, which can be attributed to the MB molecule's n-π* transitions (Veerakumar

et al., 2015). The catalytic reduction reaction was carried out at room temperature under ambient conditions. In the reduction process, the nucleophile BH^{4-} can donate electrons to the catalyst, and the electrophile MB can receive electrons from the catalyst. Thus, in a $NaBH_4$ solution, the catalyst acts as an electron relay for MB reduction.

In order to further clarify the reduction of MB in aqueous solution by NiMnOS catalysts, the color variations before and after the reaction were observed. Fresh MB solution is a blue solution. When both the catalyst and $NaBH_4$ are added to the MB solution for reaction, the test solution loses the blue color (MB) and finally becomes colorless, indicating that the MB solution has been eliminated. The course of the reaction has been tracked by using UV-Vis absorption spectrophotometry.

The strong characteristic band of MB at 664 nm was found to diminish in about 5 minutes in the presence of both NiMnOS-25 catalyst and $NaBH_4$ as shown in Figure 4.6c. The catalytic reduction of MB was also studied with only the $NaBH_4$ and without catalyst, and with the catalyst and without $NaBH_4$. With the addition of $NaBH_4$ into MB solution, the intensity of MB peak at absorption maxima of λ_{max} = 664 nm almost stayed unchanged even for a long time, indicating that the reduction process of MB does not occur in the absence of any catalysts with only $NaBH_4$ (Y. Shi et al., 2016), as shown in Figure 4.6a. The reduction of MB into Leuco-methylene blue (LMB) is thermo-dynamically feasible with only $NaBH_4$, however large energy barrier between two reactant species prevents the electron transfer from the BH_4^- donor to the MB acceptor (Hashimi et al., 2019). The reduction of MB was also not observed with only the catalyst in the absence $NaBH_4$ in the solution as shown in Figure 4.6b.

The C_t/C_o ratio as a function of reaction time for the reduction of MB on MnOS, NiOS, and NiMnOS is shown in Figure 4.6d. The MB reduction percentage of the catalyst follows the following order: NiMnOS-25> NiMnOS-50> NiMnOS-75> NiOS > MnOS. The bimetallic NiMnOS-25 had the catalytic performance with a removal percentage of about 98.47% within 5 minutes, while the degradation percentage of bare NiOS is about 9.6% within 7 minutes. The higher reduction efficiency of the catalyst could be due to the higher metal loading in the bimetal catalyst than in the single metal catalyst, the presence of a strong synergetic effect between Ni and Mn atoms, and an increase in active sites of the catalyst (Abay, Kuo, et al., 2017). From the prepared bimetal NiMnOS catalysts, NiMnOS-25 has the highest catalytic performance while NiMnOS-75 has the lowest. The lower performance of NiMnOS-75 may be attributed to the lower amount of Mn, which reduces the active sites

in the catalyst and reduces catalytic efficiency (Xueqing Li et al., 2021; J. Zhang, Yu, Zhang, Li, & Gong, 2011). As a result, the ideal Ni/Mn molar percentage is 25%, and the effectiveness of adding Ni to improve the catalyst's reduction performance has been proven.

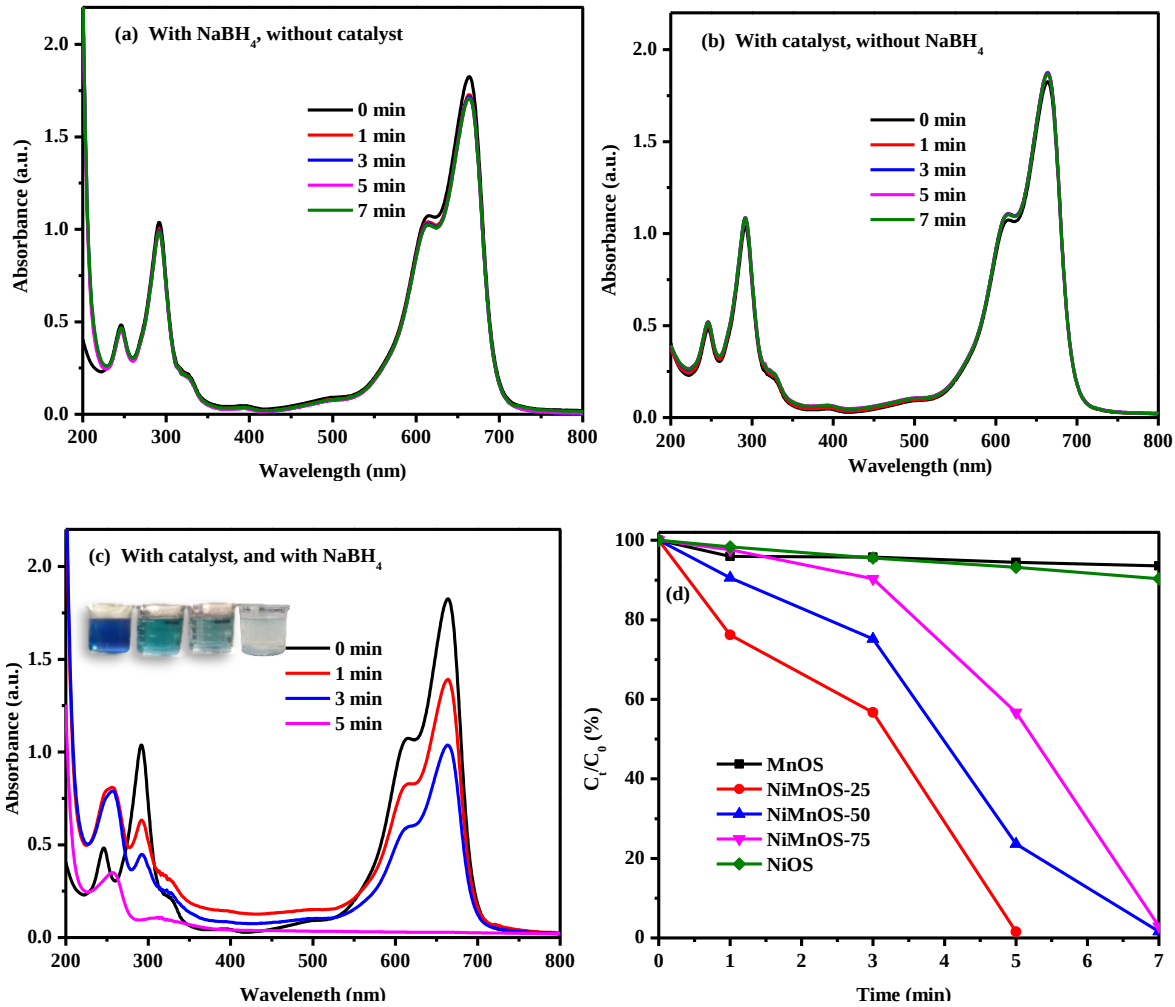

Figure 4.6. Reduction of methylene blue (MB) with (a) only $NaBH_4$, (b) only NiMnOS-25 catalyst, (c) NiMnOS-25 catalyst and with $NaBH_4$, (d) NiMnOS catalyst prepared at different molar percentages of Ni/Mn.

4.7 Reaction Kinetics

The kinetic parameters of the borohydride mediated methylene blue degradation in the presence of nickel manganese oxysulfide (NiMnOS) as a catalyst were analyzed by measuring the change in dye concentration as a function of reaction time. In order to obtain the catalytic apparent rate constant data of the methylene blue (MB) reduction reaction, the kinetics of the catalytic reduction process can be fitted using the apparent first-order rate law. Figure 4.7a shows the linear fitting results for the NiOS, NiMnOS-75, NiMnOS-50, NiMnOS-25, and MnOS catalysts. The kinetics of the reduction reaction was fitted by the apparent first-order rate equation expressed in Eqn. (4.3)

$$\ln\left(\frac{C_t}{C_o}\right) = -kt \quad \text{.....Eqn. (4.3)}$$

Where C_t is the concentration of MB (ppm) at irradiation time t (min), C_o is the initial MB (mg/l) concentration and k (min^{-1}) is the kinetic or apparent rate constant determined from the slope of the line.

The kinetic rate constants for NiOS, NiMnOS-75, NiMnOS-50, NiMnOS-25, and MnOS catalysts are displayed in Figure 4.7b. The apparent rate constant for NiMnOS-25 catalyst was $65.3\times10^{-2}\ min^{-1}$. However, the apparent rate constant values for the reduction of Mb by using NiOS, NiMnOS-75, NiMnOS-50, and MnOS were $1.4\times10^{-2}\ min^{-1}$, $33.1\times10^{-2}\ min^{-1}$, $44.2\times10^{-2}\ min^{-1}$, and $1.1\times10^{-2}\ min^{-1}$, respectively. The specific rate constant, K, in terms of $min^{-1}g^{-1}$ were measured using Eqn. (4.4).

$$K = \frac{K_{app}}{W} \quad \ldots\ldots\ldots\ldots\ldots\ldots\ldots\ldots\ldots\ldots\ldots\ldots\ldots Eqn.\ (4.4)$$

Where K_{app} is apparent rate constant, and W is total weight of the catalyst.

The NiMnOS-25 catalyst has the highest apparent rate constant of 21.8 $min^{-1}g^{-1}$. The specific rate constant (K) of NiOS, NiMnOS-75, NiMnOS-50, and MnOS were indicated in Figure 4.7b. The kinetic rate constant of different catalysts was also studied as indicated in Table 4.1.

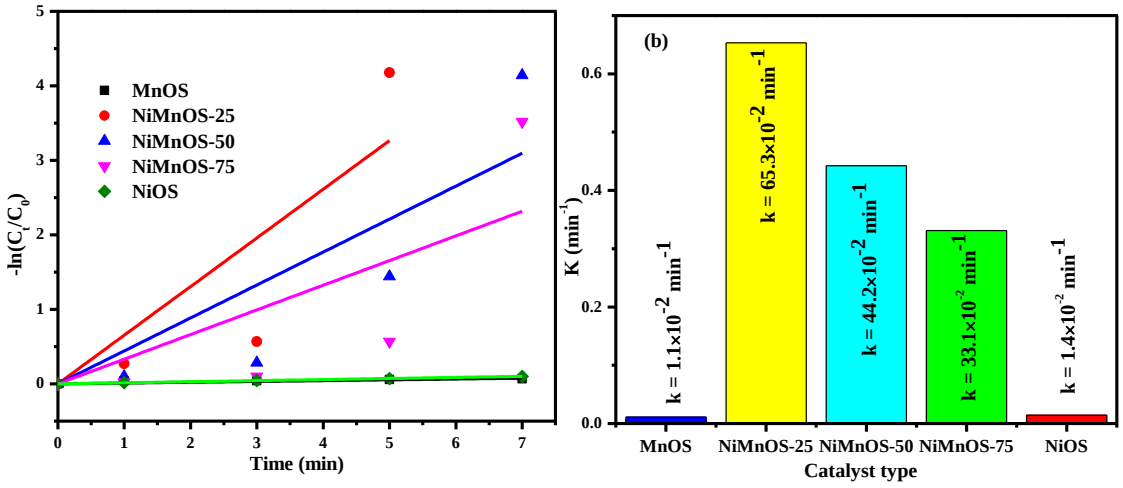

Figure 4.7. (a) Plot of -ln(C_t/C_o) versus time for reduction of methylene blue (MB) dye. (b) The kinetic rate constants for NiOS, NiMnOS-75, NiMnOS-50, NiMnOS-25 and MnOS catalysts.

Table 4.1. The kinetic rate constant of the catalysts for degradation of methylene blue

Catalysts	**Time, (min)**	**Kinetic rate constant, K_{app} (10^{-2} min^{-1})**	**Specific rate constant, K ($min^{-1}g^{-1}$)**	**Reference**
$Ag/Fe_3O_4@C$	10	0.34	0.034	(M. Zhu, Wang, Meng, & Diao, 2013)
Au/TiO_2	12	0.156	0.078	(Khan, Lee, & Cho, 2014)
$CuVOS@SiO_2$	2	0.435	87.0	(H. Sun et al., 2020)
Sn/SnO_2	210	0.132	1.32	(Das, Uddin, Rahman, & Bhoumick, 2018)
CuO-SDS	10	0.345	0.0345	(Benhadria et al., 2022)
NiOS	7	1.4	0.48	This study
NiMnOS-75	7	33.1	11.03	This study
NiMnOS-50	7	44.2	14.74	This study
NiMnOS-25	5	65.3	21.8	This study
MnOS	7	1.1	0.36	This study

4.8 Reusability and Stability of the Catalyst

In the practical uses of catalysts for the removal of the pollutant, reusability is very critical. The stability and reusability of the bimetallic oxysulfide NiMnOS-25 catalyst were further investigated by monitoring the catalytic activity during repeated reduction reactions. As a result, the reusability of our catalyst was tested by the reduction of MB for 4 runs as shown in Figure 4.8a. After the completion of each cycle reduction reaction, the catalyst was left to settle for certain times, and the upper solution is poured out. Then, the catalyst was withdrawn by centrifugation, washed with deionized water and ethanol, dried, and re-used for the next cycle. The result showed that, after 4 cycles, the bimetallic NiMnOS-25 oxysulfide catalyst maintained a good catalytic activity, which is above 96%, without deterioration. It is observed that the catalyst performs well on the following run, although it is not as excellent as the first cycle. As the amount of recycling increases, the catalyst's catalytic activity declines. The slight decrease in the performance of the catalyst is attributed to the loss of the catalyst during the recycling process. As a result, further work is required to improve the catalyst to the same level as the previous cycle (Zelekew & Kuo, 2017a).

Furthermore, after the fourth catalytic cycle of the reduction of MB, XRD analysis of the catalyst was performed to determine its stability. The XRD patterns of NiMnOS-25 before and after four cycles of MB reduction were shown in Figure 4.8b. As compared to the fresh catalyst, no obvious differences were noticed. The structure and crystalline phase of the NiMnOS-25 catalyst remained unchanged following catalytic reduction, indicating that it is stable during the reduction process and suitable for practical applications.

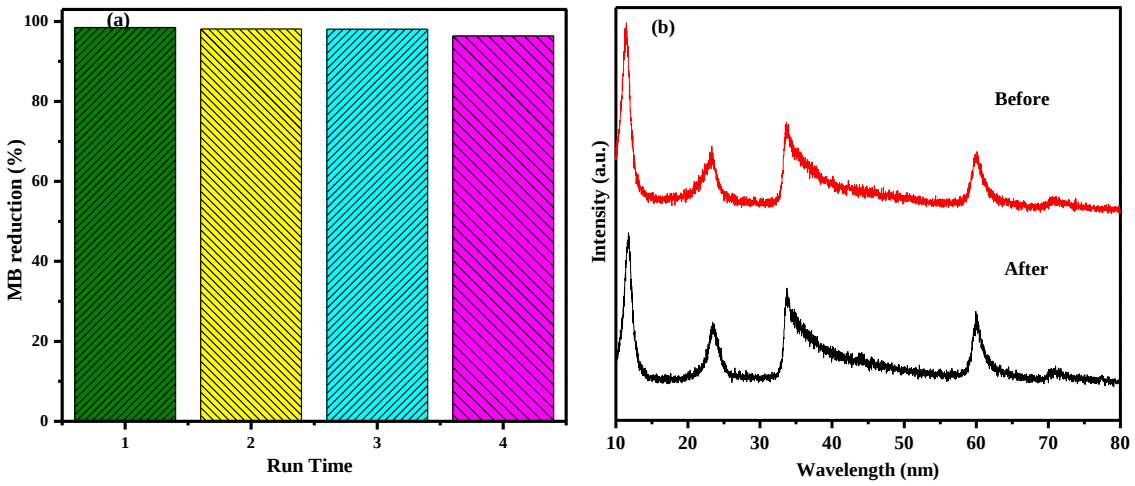

Figure 4.8. (a) Reusability of NiMnOS-25 catalyst for the reduction of MB into LMB, (b) XRD pattern of NiMnOS-25 before and after the fourth cycle.

4.9 Reaction Mechanism

According to the above-mentioned results and earlier works (Kumar & Deka, 2014; Q. Wu et al., 2021), a possible catalytic reaction mechanism for the reduction of methylene blue (MB) to Leuco-methylene blue (LMB) in the presence of $NaBH_4$ over a NiMnOS-25 catalyst was proposed as shown in Figure 4.9. First, $NaBH_4$ is dissociated in an aqueous solution and generated borohydride ions (BH_4^-). The BH_4^- ion was then adsorbed and transferred hydride ions to the surface of the catalyst (Guo et al., 2020). The hydride ions produced from $NaBH_4$ formed covalent bond with the metal ions on the surface of the NiMnOS catalysts (Xiaoyun Chen, Kuo, Zhang, Lu, Lin, et al., 2019). Subsequently, the adsorption of methylene blue (MB) on the surface of the catalyst has occurred, and strong interactions between adsorbed MB and hydride ions are formed. The reduction of methylene blue (MB) occurred via electron relay from donor species (H^-) to acceptor MB (H. Sun et al., 2020). Furthermore, as shown by the XPS analysis, the presence of Mn^{3+}, Mn^{4+}, and Ni^{2+} ions in NiMnOS catalysts boost electron transport and accelerates the reduction activity. Electron hopping transport between Mn^{3+} and Mn^{4+} in the structure help NiMnOS catalyst to provide electron for continuous electron flow in the reduction reaction (Abdeta et al., 2021; H. Li et al., 2021). Finally, due to the decreased electrostatic interaction between the catalyst and Leuco-methylene blue, the desorption of LMB from the surface of the NiMnOS-25 catalyst will spontaneously occur, resulting in a free surface for the next catalytic reduction cycle to take place (Mengqing Hu, Yan, Hu, Feng, & Zhou, 2019). Here, the catalyst serves two different purposes (Xiaoyun Chen, Kuo, Zhang, Lu, & Lin, 2019; Xiaoyun Chen, Kuo, Zhang, Lu, Lin, et al., 2019): the first is to provide an interaction center with $NaBH_4$ and organic dyes for orientation-controlled electrophilic and nucleophilic reactions; the second is to act as an electron conductor through electron transfer mechanism between Mn^{3+}/Mn^{4+}. Therefore, the reduction reaction is achieved due to both the catalyst and $NaBH_4$, which are used to release the electron and hydride ions, respectively.

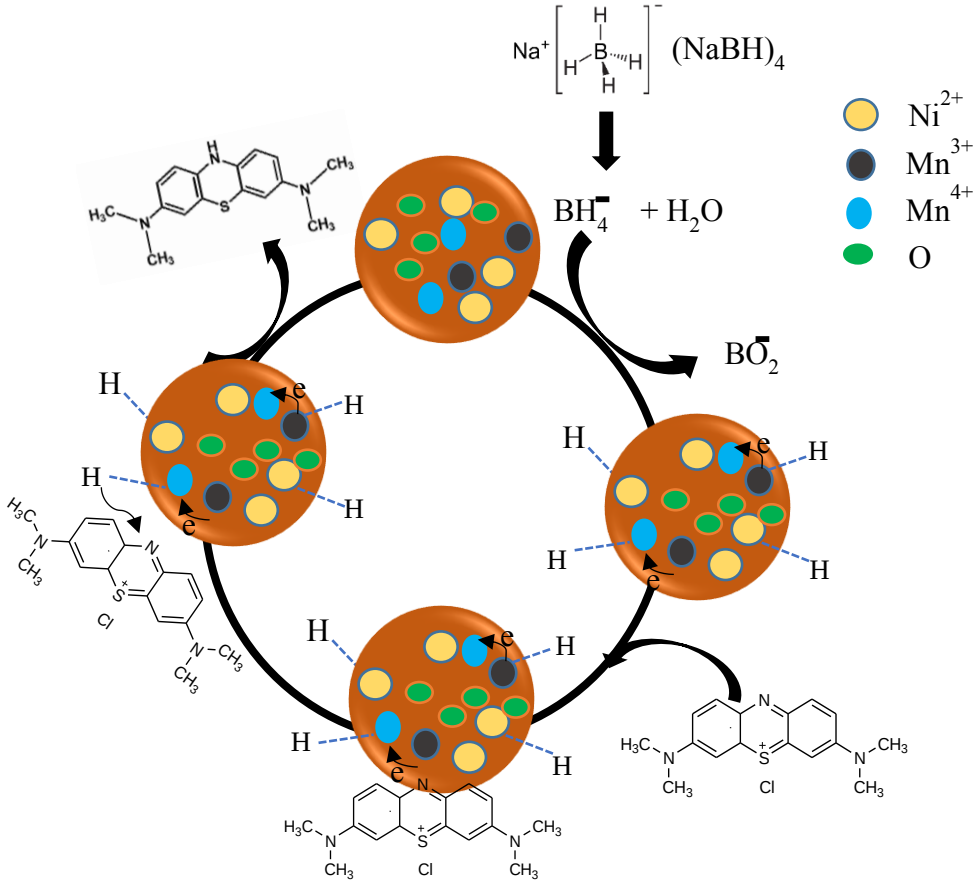

Figure 4.9. The reduction reaction mechanism of MB in presence of the NiMnOS catalyst

5. Conclusion and Recommendation

5.1 Conclusion

In this work, flower-like nickel manganese oxysulfide (NiMnOS) catalysts together with NiOS and MnOS have been prepared through a simple and environmentally friendly approach. The catalysts were successfully prepared via a facile method in a water bath at a low synthesis temperature of 90 °C. The NiMnOS catalysts showed higher activity for the reduction of methylene blue (MB) with $NaBH_4$ in an aqueous solution in comparison to the corresponding NiOS and MnOS due to the synergetic effects of Ni and Mn nanoparticles. The presence of Mn in the NiOS catalyst assists the electron relay on the catalyst to greatly enhance the performance towards the reduction of methylene blue (MB) dye. Among all the NiMnOS catalysts, the catalyst prepared with a Ni/Mn precursor molar percentage of 25:75 (NiMnOS-25) had the best catalytic activity and reduced 98.46% of MB within 5 minutes. The degradation efficiency of MB achieved by NiOS, NiMnOS-50, NiMnOS-75, and MnOS were 9.6%, 98.41%, 97.04%, and 6.40%, respectively, within 7 min. The reusability of the catalyst was also investigated and the result showed good catalytic performance after four cycles of the reduction reaction. Furthermore, the results indicate that nickel manganese oxysulfide (NiMnOS) is a promising catalyst, which is especially important for wastewater treatment targeting colored pollutants in the dye manufacturing and textile industries, due to its effective reduction performance, simple preparation, rapid reduction rate, and inexpensive cost.

5.2 Recommendation

In this work, a facile and ecofriendly synthesis method was used to prepare nickel manganese oxysulfide (NiMnOS) catalysts for the reduction of methylene blue (MB). The result showed that the catalyst has excellent reduction performance together with $NaBH_4$ in an aqueous solution. The following recommendation can be applied to make the research work completed.

1. The reduction performance of the catalyst on different organic dyes should be studied.
2. Further characterization such as TEM, BET, and EIS is needed.
3. The final product after reduction should be investigated by GC-MS and other instruments.

REFERENCE

Abay, A. K., Chen, X., & Kuo, D.-H. (2017). Highly efficient noble metal free copper nickel oxysulfide nanoparticles for catalytic reduction of 4-nitrophenol, methyl blue, and rhodamine-B organic pollutants. New Journal of Chemistry, 41(13), 5628-5638. doi:10.1039/C7NJ00676D

Abay, A. K., Kuo, D.-H., Chen, X., & Saragih, A. D. (2017). A new V-doped $Bi_2(O, S)_3$ oxysulfide catalyst for highly efficient catalytic reduction of 2-nitroaniline and organic dyes. Chemosphere, 189, 21-31.

Abdelbasir, S. M., & Shalan, A. E. (2019). An overview of nanomaterials for industrial wastewater treatment. Korean Journal of Chemical Engineering, 36(8), 1209-1225.

Abdeta, A. B., Sun, H., Guo, Y., Wu, Q., Zhang, J., Yuan, Z., . . . Chen, X. (2021). A novel AgMoOS bimetallic oxysulfide catalyst for highly efficiency catalytic reduction of organic dyes and Chromium (VI). Advanced Powder Technology, 32(8), 2856-2872.

Abdeta, A. B., Wu, Q., Kuo, D.-H., Li, P., Zhang, H., Zhang, J., . . . Chen, X. (2022). Activated carbon-supported AgMoOS bimetallic oxysulfide as a catalyst for the photocatalytic hydrogen evolution and pollutants reduction. Journal of Alloys and Compounds, 165287.

Abdullah, H., Gultom, N. S., & Kuo, D.-H. (2017). Indium oxysulfide nanosheet photocatalyst for the hexavalent chromium detoxification and hydrogen evolution reaction. Journal of Materials Science, 52(11), 6249-6264.

Abdullah, H., Gultom, N. S., & Kuo, D.-H. (2019). Synthesis and characterization of La-doped Zn (O, S) photocatalyst for green chemical detoxification of 4-nitrophenol. Journal of hazardous materials, 363, 109-118.

Abdullah, H., Gultom, N. S., Shuwanto, H., Kebede, W. L., & Kuo, D.-H. (2020). Self-Protonated Ho-Doped Zn (O, S) as a Green Chemical-Conversion Catalyst to Hydrogenate Nitro to Amino Compounds. ACS Applied Materials & Interfaces, 12(39), 43761-43770.

Abdullah, H., & Kuo, D.-H. (2019). Utilization of photocatalytic hydrogen evolved (Zn, Sn)(O, S) nanoparticles to reduce 4-nitrophenol to 4-aminophenol. International Journal of Hydrogen Energy, 44(1), 191-201.

Abdullah, H., Kuo, D.-H., & Chen, X. (2017). High efficient noble metal free Zn (O, S) nanoparticles for hydrogen evolution. International Journal of Hydrogen Energy, 42(9), 5638-5648.

Abdullah, H., Kuo, D.-H., & Gultom, N. S. (2019). N= N bond cleavage of azobenzene via photocatalytic hydrogenation with Dy-doped Zn (O, S): the progress from hydrogen evolution to green chemical conversion. Catal. Sci. Technol., 9(10), 2651-2663.

Addawiyah, E., & Gunlazuardi, J. (2018). Nickel sulfide sensitized TiO_2 nanotubes system as photo-anode: Will this system active under visible light and why? Paper presented at the AIP Conference Proceedings.

Ahmed, K. E., Kuo, D.-H., & Kebede, W. L. (2019). In-situ synthesis and characterizations of $Bi_2(O, S)_3$/Zn (O, S) composites for visible light hexavalent chromium reduction. Advanced Powder Technology, 30(8), 1664-1671.

Akbari, A., Sabouri, Z., Hosseini, H. A., Hashemzadeh, A., Khatami, M., & Darroudi, M. (2020). Effect of nickel oxide nanoparticles as a photocatalyst in dyes degradation and evaluation of effective parameters in their removal from aqueous environments. Inorganic Chemistry Communications, 115, 107867.

Al-Khalid, T., & El-Naas, M. H. (2012). Aerobic biodegradation of phenols: a comprehensive review. Critical Reviews in Environmental Science and Technology, 42(16), 1631-1690.

Alshammari, K. (2018). Heterogeneous catalysis using supported metal nanoparticles for environmental applications. Cardiff University.

Asen, P., Shahrokhian, S., & Zad, A. I. (2018). Iron-vanadium oxysulfide nanostructures as novel electrode materials for supercapacitor applications. Journal of Electroanalytical Chemistry, 818, 157-167.

Ayodhya, D., & Veerabhadram, G. (2018). A review on recent advances in photodegradation of dyes using doped and heterojunction based semiconductor metal sulfide nanostructures for environmental protection. Materials today energy, 9, 83-113.

Ba-Abbad, M. M., Kadhum, A. A. H., Mohamad, A. B., Takriff, M. S., & Sopian, K. (2012). Synthesis and catalytic activity of TiO_2 nanoparticles for photochemical oxidation of concentrated chlorophenols under direct solar radiation. Int. J. Electrochem. Sci, 7(6), 4871-4888.

Balda, R., Hakmeh, N., Merdrignac-Conanec, O., Arriandiaga, M. A., & Fernandez, J. (2017). Upconversion emission of erbium-doped lanthanum oxysulfide powders for temperature sensing. Paper presented at the Optical Components and Materials XIV.

Baruah, J. M., Kalita, S., & Narayan, J. (2019). Green chemistry synthesis of biocompatible ZnS quantum dots (QDs): their application as potential thin films and antibacterial agent. International Nano Letters, 9(2), 149-159.

Begum, R., Najeeb, J., Sattar, A., Naseem, K., Irfan, A., Al-Sehemi, A. G., & Farooqi, Z. H. (2020). Chemical reduction of methylene blue in the presence of nanocatalysts: a critical review. Reviews in Chemical Engineering, 36(6), 749-770.

Bekena, F. T., Abdullah, H., Kuo, D.-H., & Zeleke, M. A. (2019). Photocatalytic reduction of 4-nitrophenol using effective hole scavenger over novel Mg-doped Zn (O, S) nanoparticles. Journal of Industrial and Engineering Chemistry, 78, 116-124.

Bekena, F. T., Kuo, D.-H., & Kebede, W. L. (2020). Universal and highly efficient degradation performance of novel $Bi_2(O, S)_3/Mo(O, S)_2$ nanocomposite photocatalyst under visible light. Separation and Purification Technology, 247, 117042.

Benhadria, N., Hachemaoui, M., Zaoui, F., Mokhtar, A., Boukreris, S., Attar, T., . . . Boukoussa, B. (2022). Catalytic reduction of methylene blue dye by copper oxide nanoparticles. Journal of Cluster Science, 33(1), 249-260.

Bokare, A. D., Chikate, R. C., Rode, C. V., & Paknikar, K. M. (2008). Iron-nickel bimetallic nanoparticles for reductive degradation of azo dye Orange G in aqueous solution. Applied Catalysis B: Environmental, 79(3), 270-278.

Bollard, M. E., Keun, H. C., Beckonert, O., Ebbels, T. M., Antti, H., Nicholls, A. W., . . . Lindon, J. C. (2005). Comparative metabonomics of differential hydrazine toxicity in the rat and mouse. Toxicology and applied pharmacology, 204(2), 135-151.

Chaki, S. H., Chauhan, S. M., Tailor, J. P., & Deshpande, M. P. (2017). Synthesis of manganese sulfide (MnS) thin films by chemical bath deposition and their characterization. Journal of materials research and technology, 6(2), 123-128.

Chan, S. H. S., Yeong Wu, T., Juan, J. C., & Teh, C. Y. (2011). Recent developments of metal oxide semiconductors as photocatalysts in advanced oxidation processes (AOPs) for treatment of dye waste-water. Journal of Chemical Technology & Biotechnology, 86(9), 1130-1158.

Chandrasekaran, S., Yao, L., Deng, L., Bowen, C., Zhang, Y., Chen, S., . . . Zhang, P. (2019). Recent advances in metal sulfides: from controlled fabrication to electrocatalytic, photocatalytic and photoelectrochemical water splitting and beyond. Chemical Society Reviews, 48(15), 4178-4280.

Chen, H., Wu, Z., Zheng, Z., Chen, T., Guo, X., Li, J., & Zhong, B. (2018). Tuning the component ratio and corresponding sodium storage properties of layer-tunnel hybrid $Na_{0.6}Mn_{1-x}Ni_xO_2$ cathode by a simple cationic Ni^{2+} doping strategy. Electrochimica Acta, 273, 63-70.

Chen, H., Zhong, A., Wu, J., Zhao, J., & Yan, H. (2012). Adsorption Behaviors and Mechanisms of Methyl Orange on Heat-Treated Palygorskite Clays. Industrial & Engineering Chemistry Research, 51(43), 14026-14036. doi:10.1021/ie300702j

Chen, S. S., Huang, Y. C., & Chen, T. Y. (2014). Reduction of hexavalent chromium in water using iron-aluminum bimetallic particles. Paper presented at the Advanced Materials Research.

Chen, X., Abdullah, H., Kuo, D.-H., Huang, H.-N., & Fang, C.-C. (2017). Abiotic synthesis with the CC bond formation in ethanol from CO_2 over (Cu, M)(O, S) catalysts with M= Ni, Sn, and Co. Scientific reports, 7(1), 1-8.

Chen, X., He, Y., Zhang, Q., Li, L., Hu, D., & Yin, T. (2010). Fabrication of sandwich-structured ZnO/reduced graphite oxide composite and its photocatalytic properties. Journal of Materials Science, 45(4), 953-960.

Chen, X., & Kuo, D.-H. (2017). Nanoflower bimetal CuInOS oxysulfide catalyst for the reduction of Cr (VI) in the dark. ACS Sustainable Chemistry & Engineering, 5(5), 4133-4143.

Chen, X., Kuo, D.-H., Saragih, A. D., Wu, Z.-Y., Abdullah, H., & Lin, J. (2019). The effect of the Cu^{+}/Cu^{2+} ratio on the redox reactions by nanoflower CuNiOS catalysts. Chemical Engineering Science, 194, 105-115.

Chen, X., Kuo, D.-H., Wu, Z.-Y., Zhang, J., Guo, Y., Sun, H., & Lin, J. (2019). Multi-component (Cu, Mn)(Se, S) nanosheet catalysts for redox reactions in the dark. Separation and Purification Technology, 211, 71-80.

Chen, X., Kuo, D.-H., Zhang, J., Lu, Q., & Lin, J. (2019). Nanosheet bimetal oxysulfide CuSbOS catalyst for highly efficient catalytic reduction of heavy metal ions and organic dyes. Journal of Molecular Liquids, 275, 204-214.

Chen, X., Kuo, D. H., Zhang, J., Lu, Q., Lin, J., & Liao, Y. (2019). Tubular bimetal oxysulfide CuMgOS catalyst for rapid reduction of heavy metals and organic dyes. Applied Organometallic Chemistry, 33(4), e4824.

Chen, X., Sun, H., Zhang, J., Guo, Y., & Kuo, D.-H. (2019). Cationic S-doped TiO_2/SiO_2 visible-light photocatalyst synthesized by co-hydrolysis method and its application for organic degradation. Journal of Molecular Liquids, 273, 50-57.

Cheng, B., Le, Y., Cai, W., & Yu, J. (2011). Synthesis of hierarchical Ni $(OH)_2$ and NiO nanosheets and their adsorption kinetics and isotherms to Congo red in water. Journal of hazardous materials, 185(2-3), 889-897.

Cockayne, E., & Li, L. (2012). First-principles DFT+ U studies of the atomic, electronic, and magnetic structure of α-MnO_2 (cryptomelane). Chemical Physics Letters, 544, 53-58.

Das, O., Uddin, M., Rahman, M., & Bhoumick, M. (2018). Highly active carbon supported Sn/SnO_2 photocatalysts for degrading organic dyes. Paper presented at the Journal of Physics: Conference Series.

Do, H. H., Nguyen, D. L. T., Nguyen, X. C., Le, T.-H., Nguyen, T. P., Trinh, Q. T., . . . Van Le, Q. (2020). Recent progress in TiO_2-based photocatalysts for hydrogen evolution reaction: A review. Arabian Journal of Chemistry, 13(2), 3653-3671.

Dong, B., Li, W., Huang, X., Ali, Z., Zhang, T., Yang, Z., & Hou, Y. (2019). Fabrication of hierarchical hollow Mn doped Ni $(OH)_2$ nanostructures with enhanced catalytic activity towards electrochemical oxidation of methanol. Nano Energy, 55, 37-41.

Dube, S., Moutloali, R., & Malinga, S. (2020). Hyperbranched polyethyleneimine/multi-walled carbon nanotubes polyethersulfone membrane incorporated with Fe-Cu bimetallic nanoparticles for water treatment. Journal of Environmental Chemical Engineering, 8(4), 103962.

Dubois, V., Pecquenard, B., Soulé, S., Martinez, H., & Le Cras, F. (2017). Dual cation-and anion-based redox process in lithium titanium oxysulfide thin film cathodes for all-solid-state lithium-ion batteries. ACS Applied Materials & Interfaces, 9(3), 2275-2284.

Eastman, E., Brewer, L., Bromley, L. A., Gilles, P. W., & Lofgren, N. L. (1951). Preparation and Properties of the Oxide-Sulfides of Cerium, Zirconium, Thorium and Uranium2. Journal of the American Chemical Society, 73(8), 3896-3898.

Ethiraj, A. S., Uttam, P., Varunkumar, K., Chong, K. F., & Ali, G. A. (2020). Photocatalytic performance of a novel semiconductor nanocatalyst: Copper doped nickel oxide for phenol degradation. Materials Chemistry and Physics, 242, 122520.

Fu, F., Cheng, Z., & Lu, J. (2015). Synthesis and use of bimetals and bimetal oxides in contaminants removal from water: a review. RSC Advances, 5(104), 85395-85409. doi:10.1039/C5RA13067K

Fujishima, A., & Honda, K. (1972). Electrochemical photolysis of water at a semiconductor electrode. nature, 238(5358), 37-38.

Gholipour, M. R., Dinh, C.-T., Béland, F., & Do, T.-O. (2015). Nanocomposite heterojunctions as sunlight-driven photocatalysts for hydrogen production from water splitting. Nanoscale, 7(18), 8187-8208.

Gnanasekaran, L., Hemamalini, R., Saravanan, R., Ravichandran, K., Gracia, F., Agarwal, S., & Gupta, V. K. (2017). Synthesis and characterization of metal oxides (CeO2, CuO, NiO, Mn3O4, SnO2 and ZnO) nanoparticles as photo catalysts for degradation of textile dyes. Journal of Photochemistry and Photobiology B: Biology, 173, 43-49.

Gong, C., Chen, F., Yang, Q., Luo, K., Yao, F., Wang, S., . . . Wang, D. (2017). Heterogeneous activation of peroxymonosulfate by Fe-Co layered doubled hydroxide for efficient catalytic degradation of Rhoadmine B. Chemical Engineering Journal, 321, 222-232.

Gultom, N. S., Abdullah, H., & Kuo, D.-H. (2017). Enhanced photocatalytic hydrogen production of noble-metal free Ni-doped Zn (O, S) in ethanol solution. International Journal of Hydrogen Energy, 42(41), 25891-25902.

Gultom, N. S., Abdullah, H., Kuo, D.-H., & Ke, W.-C. (2019). Oriented p–n heterojunction Ag2O/Zn (O, S) nanodiodes on mesoporous SiO2 for photocatalytic hydrogen production. ACS Applied Energy Materials, 2(5), 3228-3236.

Guo, Y., Zelekew, O. A., Sun, H., Kuo, D.-H., Lin, J., & Chen, X. (2020). Catalytic reduction of organic and hexavalent chromium pollutants with highly active bimetal CuBiOS oxysulfide catalyst under dark. Separation and Purification Technology, 242, 116769.

Han, Y., Chen, C., Li, Y., Zhou, L., Lan, Y., & Li, Y. (2019). Preparation of Cu-Y binary oxysulfide and its application in the removal of arsenic from aqueous solutions. Separation and Purification Technology, 213, 410-418.

Hashimi, A. S., Nohan, M. A. N. M., Chin, S. X., Zakaria, S., & Chia, C. H. (2019). Rapid catalytic reduction of 4-nitrophenol and clock reaction of methylene blue using copper nanowires. Nanomaterials, 9(7), 936.

Hayashi, A., Komiya, R., Tatsumisago, M., & Minami, T. (2002). Characterization of Li2S–SiS2–Li3MO3 (M= B, Al, Ga and In) oxysulfide glasses and their application to solid state lithium secondary batteries. Solid State Ionics, 152, 285-290.

Honarmand, M., Golmohammadi, M., & Naeimi, A. (2019). Biosynthesis of tin oxide (SnO2) nanoparticles using jujube fruit for photocatalytic degradation of organic dyes. Advanced Powder Technology, 30(8), 1551-1557.

Hu, H., Xin, J. H., Hu, H., Wang, X., Miao, D., & Liu, Y. (2015). Synthesis and stabilization of metal nanocatalysts for reduction reactions–a review. Journal of Materials Chemistry A, 3(21), 11157-11182.

Hu, M., Liu, Y., Yao, Z., Ma, L., & Wang, X. (2018). Catalytic reduction for water treatment. Frontiers of Environmental Science & Engineering, 12(1), 1-18.

Hu, M., Yan, X., Hu, X., Feng, R., & Zhou, M. (2019). Synthesis of silver decorated silica nanoparticles with rough surfaces as adsorbent and catalyst for methylene blue removal. Journal of Sol-Gel Science and Technology, 89(3), 754-763.

Huerta-Flores, A. M., Torres-Martínez, L. M., Moctezuma, E., Singh, A. P., & Wickman, B. (2018). Green synthesis of earth-abundant metal sulfides (FeS2, CuS, and NiS2) and their use as visible-light active photocatalysts for H_2 generation and dye removal. Journal of Materials Science: Materials in Electronics, 29(13), 11613-11626.

Islam, M. S., & Tanaka, M. (2004). Impacts of pollution on coastal and marine ecosystems including coastal and marine fisheries and approach for management: a review and synthesis. Marine pollution bulletin, 48(7-8), 624-649.

Jafari, H., & Afshar, S. (2016). Improved photodegradation of organic contaminants using nano-TiO_2 and TiO_2–SiO_2 deposited on Portland cement concrete blocks. Photochemistry and photobiology, 92(1), 87-101.

Jansi Rani, B., Dhivya, N., Ravi, G., Zance, S. S., Yuvakkumar, R., & Hong, S. I. (2019). Electrochemical performance of β-Nis@ Ni $(OH)_2$ nanocomposite for water splitting applications. Acs Omega, 4(6), 10302-10310.

Jawad, A., Lu, X., Chen, Z., & Yin, G. (2014). Degradation of chlorophenols by supported Co–Mg–Al layered double hydrotalcite with bicarbonate activated hydrogen peroxide. The Journal of Physical Chemistry A, 118(43), 10028-10035.

Jia, D., Gao, H., Dong, W., Fan, S., Dang, R., & Wang, G. (2017). Hierarchical α-Ni (OH) 2 composed of ultrathin nanosheets with controlled interlayer distances and their enhanced catalytic performance. ACS Applied Materials & Interfaces, 9(24), 20476-20483.

Jiang, G., Wei, X., Chen, Y., Duan, C., Yin, M., Yang, B., & Cao, W. (2015). Luminescent La_2O_2S: Eu^{3+} nanoparticles as non-contact optical temperature sensor in physiological temperature range. Materials Letters, 143, 98-100.

Jiang, G., Wei, X., Zhou, S., Chen, Y., Duan, C., & Yin, M. (2014). Neodymium doped lanthanum oxysulfide as optical temperature sensors. Journal of luminescence, 152, 156-159.

Jiang, L., Li, Y., Wu, X., & Zhang, G. (2021). Rich oxygen vacancies mediated bismuth oxysulfide crystals towards photocatalytic CO_2-to-CH_4 conversion. Science China Materials, 64(9), 2230-2241.

Junaid, M., Imran, M., Ikram, M., Naz, M., Aqeel, M., Afzal, H., . . . Ali, S. (2019). The study of Fe-doped CdS nanoparticle-assisted photocatalytic degradation of organic dye in wastewater. Applied Nanoscience, 9(8), 1593-1602.

Kassem, A. A., Abdelhamid, H. N., Fouad, D. M., & Ibrahim, S. A. (2021). Catalytic reduction of 4-nitrophenol using copper terephthalate frameworks and CuO@ C composite. Journal of Environmental Chemical Engineering, 9(1), 104401.

Kaur, B., Raza, R., & Branda, N. R. (2021). A dual-mode visual detector for toxic hydrazine. RSC Advances, 11(37), 22835-22841.

Kebede, W. L., Kuo, D.-H., Bekena, F. T., & Duresa, L. W. (2020). Highly efficient In–Mo (O, S)$_2$ oxy-sulfide for degradation of organic pollutants under visible light irradiation: An example of photocatalyst on its dye selectivity. Chemosphere, 254, 126823.

Kebede, W. L., Kuo, D.-H., Zeleke, M. A., & Ahmed, K. E. (2019). A novel Sb-doped Mo (O, S)$_3$ oxy-sulfide photocatalyst for degradation of methylene blue dye under visible light irradiation. Journal of Alloys and Compounds, 797, 986-994.

Khan, M. M., Lee, J., & Cho, M. H. (2014). Au@ TiO_2 nanocomposites for the catalytic degradation of methyl orange and methylene blue: an electron relay effect. Journal of Industrial and Engineering Chemistry, 20(4), 1584-1590.

Kim, C., Doh, S. J., Lee, S. G., Lee, S. J., & Kim, H. Y. (2007). Visible-light absorptivity of a zincoxysulfide (ZnO_xS_{1-x}) composite semiconductor and its photocatalytic activities for degradation of organic pollutants under visible-light irradiation. Applied Catalysis A: General, 330, 127-133.

Kong, X., Zhu, H., Chen, C., Huang, G., & Chen, Q. (2017). Insights into the reduction of 4-nitrophenol to 4-aminophenol on catalysts. Chemical Physics Letters, 684, 148-152.

Kuai, Y., Liu, M., Wang, T., Fu, Y., Ma, H., Jiang, Q., . . . Hu, K. (2017). Sea anemone-like zinc-cobalt oxysulfides grown on Ni foam as a battery-type electrode with admirable performance. Ionics, 23(6), 1391-1398.

Kumar, M., & Deka, S. (2014). Multiply twinned AgNi alloy nanoparticles as highly active catalyst for multiple reduction and degradation reactions. ACS Applied Materials & Interfaces, 6(18), 16071-16081.

Larquet, C., & Carenco, S. (2020). Metal Oxysulfides: From Bulk Compounds to Nanomaterials. Frontiers in Chemistry, 8(179). doi:10.3389/fchem.2020.00179

Lewis, E., O'Keeffe, S., Grattan, M., Hounsell, A., McCarthy, D., Woulfe, P., . . . Santhanam, A. (2014). Terbium-doped gadolinium oxysulfide (Gd_2O_2S: Tb) scintillation-based polymer optical fibre sensor for real time monitoring of radiation dose in oncology. Paper presented at the Optical Sensing and Detection III.

Li, H., Zhang, H., Thayil, S., Chang, A., Sang, X., & Ma, X. (2021). Enhanced aging and thermal shock performance of Mn1. 95− xCO0. 21Ni0. 84SrxO4 NTC ceramics. Journal of Advanced Ceramics, 10(2), 258-270.

Li, J., Wei, M., Chu, W., & Wang, N. (2017). High-stable α-phase NiCo double hydroxide microspheres via microwave synthesis for supercapacitor electrode materials. Chemical Engineering Journal, 316, 277-287.

Li, W., Wang, Z., Liao, H., Liu, X., Zhou, L., Lan, Y., & Zhang, J. (2021). Enhanced degradation of 2, 4, 6-trichlorophenol by activated peroxymonosulfate with sulfur doped copper manganese bimetallic oxides. Chemical Engineering Journal, 417, 128121.

Li, X.-y., Cui, Y.-h., Feng, Y.-j., Xie, Z.-m., & Gu, J.-D. (2005). Reaction pathways and mechanisms of the electrochemical degradation of phenol on different electrodes. Water research, 39(10), 1972-1981.

Li, X., Chen, D., Li, N., Xu, Q., Li, H., He, J., & Lu, J. (2021). One-step fabrication of bimetallic CuCoOS as an efficient catalyst for Cr (vi) reduction. Environmental Science: Nano, 8(9), 2453-2463.

Li, X., Zhang, L., Wang, Z., Wu, S., & Ma, J. (2021). Cellulose controlled zinc oxide nanoparticles with adjustable morphology and their photocatalytic performances. Carbohydrate Polymers, 259, 117752.

Li, Y., Dong, H., Li, L., Tang, L., Tian, R., Li, R., . . . Xiao, J. (2021). Recent advances in waste water treatment through transition metal sulfides-based advanced oxidation processes. Water research, 192, 116850.

Lim, J. S., Saldana-Greco, D., & Rappe, A. M. (2016). Improved pseudopotential transferability for magnetic and electronic properties of binary manganese oxides from DFT+ U+ J calculations. Physical Review B, 94(16), 165151.

Lin, Z., Lu, Y., & Huang, J. (2019). A hierarchical Ag2O-nanoparticle/TiO2-nanotube composite derived from natural cellulose substance with enhanced photocatalytic performance. Cellulose, 26(11), 6683-6700.

Liu, L. (2013). Nano-aggregates of cobalt nickel oxysulfide as a high-performance electrode material for supercapacitors. Nanoscale, 5(23), 11615-11619.

Liu, M., Fu, Y., Ma, H., Wang, T., Guan, C., & Hu, K. (2016). Flower-like manganese-cobalt oxysulfide supported on Ni foam as a novel faradaic electrode with commendable performance. Electrochimica Acta, 191, 916-922.

Liu, Y., Zhang, Y., Kou, Q., Chen, Y., Han, D., Wang, D., . . . Xing, S. (2018). Eco-friendly seeded Fe 3 O 4-Ag nanocrystals: A new type of highly efficient and low cost catalyst for methylene blue reduction. RSC Advances, 8(4), 2209-2218.

Lu, X., Wang, G., Xie, S., Shi, J., Li, W., Tong, Y., & Li, Y. (2012). Efficient photocatalytic hydrogen evolution over hydrogenated ZnO nanorod arrays. Chemical Communications, 48(62), 7717-7719.

Luo, X., Hu, H., Pan, Z., Pei, F., Qian, H., Miao, K., . . . Feng, G. (2020). Efficient and stable catalysis of hollow Cu9S5 nanospheres in the Fenton-like degradation of organic dyes. Journal of hazardous materials, 396, 122735.

Mahmood, T., Momin, S., Ali, R., Naeem, A., & Khan, A. (2022). Technologies for Removal of Emerging Contaminants from Wastewater.

Manu, B., & Chaudhari, S. (2002). Anaerobic decolorisation of simulated textile wastewater containing azo dyes. Bioresource technology, 82(3), 225-231.

Marcì, G., & Palmisano, L. (2019). Heterogeneous Photocatalysis: Relationships with Heterogeneous Catalysis and Perspectives: Elsevier.

Martínez-Sánchez, C., Regmi, C., Lee, S., & Rodríguez-González, V. (2021). Effects of Ce doping on the photocatalytic and electrochemical performance of nickel hydroxide nanostructures. Topics in Catalysis, 64(1), 73-83.

Martínez-Vargas, B. L., Cruz-Ramírez, M., Díaz-Real, J. A., Rodríguez-López, J., Bacame-Valenzuela, F. J., Ortega-Borges, R., . . . Ortiz-Frade, L. (2019). Synthesis and characterization of n-ZnO/p-MnO nanocomposites for the photocatalytic degradation of anthracene. Journal of Photochemistry and Photobiology A: Chemistry, 369, 85-96.

Mazaheri, H., Ghaedi, M., Asfaram, A., & Hajati, S. (2016). Performance of CuS nanoparticle loaded on activated carbon in the adsorption of methylene blue and bromophenol blue dyes in binary aqueous solutions: using ultrasound power and optimization by central composite design. Journal of Molecular Liquids, 219, 667-676.

Mohammad, A., Khan, M. E., & Cho, M. H. (2020). Sulfur-doped-graphitic-carbon nitride (Sg-C3N4) for low cost electrochemical sensing of hydrazine. Journal of Alloys and Compounds, 816, 152522.

Mohapatra, L., & Parida, K. (2012). Zn–Cr layered double hydroxide: visible light responsive photocatalyst for photocatalytic degradation of organic pollutants. Separation and Purification Technology, 91, 73-80.

Munyai, S., & Hintsho-Mbita, N. C. (2021). Green derived metal sulphides as photocatalysts for waste water treatment. A review. Current research in green and sustainable chemistry, 2021 v.4, pp. 100163-. doi:10.1016/j.crgsc.2021.100163

Nagajyothi, P., Deyarayapalli, K., Tettey, C., Vattikuti, S. P., & Shim, J. (2019). Eco-friendly green synthesis: catalytic activity of nickel hydroxide nanoparticles. Materials Research Express, 6(5), 055036.

Nagarajan, D., & Venkatanarasimhan, S. (2019). Copper (II) oxide nanoparticles coated cellulose sponge—an effective heterogeneous catalyst for the reduction of toxic organic dyes. Environmental Science and Pollution Research, 26(22), 22958-22970.

Najeeb, J., Ahmad, G., Nazir, S., Naseem, K., & Kanwal, A. (2021). Critical analysis of various supporting mediums employed for the incapacitation of silver nanomaterial for aniline and phenolic pollutants: a review. Korean Journal of Chemical Engineering, 38(2), 248-263.

Naz, M., Rafiq, A., Ikram, M., Haider, A., Ahmad, S. O. A., Haider, J., & Naz, S. (2021). Elimination of dyes by catalytic reduction in the absence of light: A review. Journal of Materials Science, 56(28), 15572-15608.

Nishioka, S., Kanazawa, T., Shibata, K., Tsujimoto, Y., zur Loye, H.-C., & Maeda, K. (2019). A zinc-based oxysulfide photocatalyst $SrZn_2S_2O$ capable of reducing and oxidizing water. Dalton Transactions, 48(42), 15778-15781. doi:10.1039/C9DT03699G

Oriakhi, C. O., Farr, I. V., & Lerner, M. M. (1996). Incorporation of poly (acrylic acid), poly (vinylsulfonate) and poly (styrenesulfonate) within layered double hydroxides. Journal of Materials Chemistry, 6(1), 103-107.

Ouvrard, G., Tchangbédji, G., Deniard, P., & Prouzet, E. (1995). Structural, physical and electrochemical characteristics of a vanadium oxysulfide, a cathode material for lithium batteries. Journal of power sources, 54(2), 246-249.

Pandey, S. K., Pandey, S., Pandey, A. C., & Mehrotra, G. (2013). Zinc oxysulfide ternary alloy nanocrystals: A bandgap modulated photocatalyst. Applied Physics Letters, 102(23), 233110.

Pandya, A., Pandya, C., & Dave, B. (2018). Biodegradation of toxic dyes and textile dye effluent–a review. Development, 5(03).

Park, S. H., Sun, Y.-K., Park, K. S., Nahm, K. S., Lee, Y. S., & Yoshio, M. (2002). Synthesis and electrochemical properties of lithium nickel oxysulfide ($LiNiS_yO_{2-y}$) material for lithium secondary batteries. Electrochimica Acta, 47(11), 1721-1726.

Poul, L., Jouini, N., & Fiévet, F. (2000). Layered hydroxide metal acetates (metal= zinc, cobalt, and nickel): elaboration via hydrolysis in polyol medium and comparative study. Chemistry of materials, 12(10), 3123-3132.

Pouretedal, H. R., Norozi, A., Keshavarz, M. H., & Semnani, A. (2009). Nanoparticles of zinc sulfide doped with manganese, nickel and copper as nanophotocatalyst in the degradation of organic dyes. Journal of hazardous materials, 162(2-3), 674-681.

Pradeep, T. (2009). Noble metal nanoparticles for water purification: a critical review. Thin solid films, 517(24), 6441-6478.

Quiton, K. G. N., Lu, M., & Huang, Y. H. (2021). Synthesis and catalytic utilization of bimetallic systems for wastewater remediation: A review. Chemosphere, 262, 128371.

Ramulu, B., Arbaz, S. J., & Yu, J. S. (2022). Efficient Co–Ni oxysulfide nanoarchitectured materials for long-lasting electrochemical cells: Biodegradable parafilm assisted pouch-type cells for portable electronic applications. Composites Part B: Engineering, 238, 109915.

Ran, S., Zhu, Y., Huang, H., Liang, B., Xu, J., Liu, B., . . . Ye, J. (2012). Phase-controlled synthesis of 3D flower-like Ni $(OH)_2$ architectures and their applications in water treatment. CrystEngComm, 14(9), 3063-3068.

Ranjith, K. S., Raju, G. S. R., Kwak, C. H., Ghoreishian, S. M., Huh, Y. S., Im, J. S., & Han, Y. K. (2021). Metal-organic framework-derived carbon-cobalt oxysulfide nanocage heterostructure electrode for efficient hybrid supercapacitors. International Journal of Energy Research, 45(4), 5988-6001.

Ravindhranath, K., & Ramamoorty, M. (2017). Nickel based nano particles as adsorbents in water purification methods-a review. Oriental Journal of Chemistry, 33(4), 1603.

Ren, J., Jiang, L., Li, Y., & Zhang, G. (2021). Cobalt doped bismuth oxysulfide with abundant oxygen vacancies towards tetracycline degradation through peroxymonosulfate activation. Separation and Purification Technology, 119100.

Rojas, S., & Horcajada, P. (2020). Metal–organic frameworks for the removal of emerging organic contaminants in water. Chemical Reviews, 120(16), 8378-8415.

Saeed, M., Usman, M., & ul Haq, A. (2018). Catalytic Degradation of Organic Dyes in Aqueous Medium (Vol. 13): IntechOpen London, UK.

Saikia, P., Miah, A. T., & Das, P. P. (2017). Highly efficient catalytic reductive degradation of various organic dyes by Au/CeO 2-TiO 2 nano-hybrid. Journal of Chemical Sciences, 129(1), 81-93.

Samanta, S. K., Maiti, K., Ali, S. S., Guria, U. N., Ghosh, A., Datta, P., & Mahapatra, A. K. (2020). A solvent directed D-π-A fluorescent chemodosimeter for selective detection of hazardous hydrazine in real water sample and living cell. Dyes and Pigments, 173, 107997.

Sanyal, T., Bhattacharjee, P., Paul, S., & Bhattacharjee, P. (2020). Recent advances in arsenic research: significance of differential susceptibility and sustainable strategies for mitigation. Frontiers in public health, 8, 464.

Sarma, P. V., Vineesh, T. V., Kumar, R., Sreepal, V., Prasannachandran, R., Singh, A. K., & Shaijumon, M. M. (2020). Nanostructured tungsten oxysulfide as an efficient electrocatalyst for hydrogen evolution reaction. ACS Catalysis, 10(12), 6753-6762.

Schellekens, J., Heidecke, L., Nguyen, N., & Spit, W. (2018). The economic value of water–water as a key resource for economic growth in the EU. Rotterdam: ECORYS.

Seger, B., Laursen, A. B., Vesborg, P. C., Pedersen, T., Hansen, O., Dahl, S., & Chorkendorff, I. (2012). Hydrogen production using a molybdenum sulfide catalyst on a titanium-protected n+ p-silicon photocathode. Angewandte Chemie, 124(36), 9262-9265.

Senobari, S., & Nezamzadeh-Ejhieh, A. (2018). A comprehensive study on the enhanced photocatalytic activity of CuO-NiO nanoparticles: designing the experiments. Journal of Molecular Liquids, 261, 208-217.

Serrà, A., Zhang, Y., Sepúlveda, B., Gómez, E., Nogués, J., Michler, J., & Philippe, L. (2019). Highly active ZnO-based biomimetic fern-like microleaves for photocatalytic water decontamination using sunlight. Applied Catalysis B: Environmental, 248, 129-146.

Sharrouf, M., Awad, R., Roumié, M., & Marhaba, S. (2015). Structural, optical and room temperature magnetic study of Mn_2O_3 nanoparticles. Materials Sciences and Applications, 6(10), 850.

Shi, M., Qiu, T., Tang, B., Zhang, G., Yao, R., Xu, W., . . . Peng, J. (2021). Temperature-controlled crystal size of wide band gap nickel oxide and its application in electrochromism. Micromachines, 12(1), 80.

Shi, Y., Zhang, X., Zhu, Y., Tan, H., Chen, X., & Lu, Z.-H. (2016). Core–shell structured nanocomposites Ag@ CeO_2 as catalysts for hydrogenation of 4-nitrophenol and 2-nitroaniline. RSC Advances, 6(53), 47966-47973.

Shu, Q. W., Lan, J., Gao, M. X., Wang, J., & Huang, C. Z. (2015). Controlled synthesis of CuS caved superstructures and their application to the catalysis of organic dye degradation in the absence of light. CrystEngComm, 17(6), 1374-1380.

Shultz, L. R., Hu, L., Preradovic, K., Beazley, M. J., Feng, X., & Jurca, T. (2019). A broader-scope analysis of the catalytic reduction of nitrophenols and azo dyes with noble metal nanoparticles. ChemCatChem, 11(11), 2590-2595.

Shuwanto, H., Gultom, N. S., Abdullah, H., & Kuo, D.-H. (2020). Environmentally Benign Photoreactions for Hydrogen Production and Cleavage of N═ N bond in Azobenzene over Co-Doped Zn (O, S) Nanocatalyst: The Role of In Situ Generated H+. ACS Applied Energy Materials, 3(12), 12692-12702.

Singh, B., Kaur, J., & Singh, K. (2012). Microbial remediation of explosive waste. Critical reviews in microbiology, 38(2), 152-167.

Singh, C., Goyal, A., & Singhal, S. (2014). Nickel-doped cobalt ferrite nanoparticles: efficient catalysts for the reduction of nitroaromatic compounds and photo-oxidative degradation of toxic dyes. Nanoscale, 6(14), 7959-7970.

Sinha, S., Ramasamy, H. V., Nandi, D. K., Didwal, P. N., Cho, J. Y., Park, C.-J., . . . Heo, J. (2018). Atomic layer deposited zinc oxysulfide anodes in Li-ion batteries: an efficient solution for electrochemical instability and low conductivity. Journal of Materials Chemistry A, 6(34), 16515-16528.

Sisay, G., Abdullah, H., Kuo, D.-H., Lakew, W., Shuwanto, H., & Fentie, S. (2021). Zn-Ce-Ga trimetal oxysulfide as a dual-functional catalyst: Hydrogen evolution and hydrogenation reactions in a mild condition. Applied Surface Science, 563, 150383.

Smedley, P. L., & Kinniburgh, D. G. (2001). Source and behaviour of arsenic in natural waters. United Nations synthesis report on arsenic in drinking water. World Health Organization, Geneva, Switzerland. http://www. who. int/water_sanitation_health/dwq/arsenicun1. pdf, 1-61.

Sohrabnezhad, S., Pourahmad, A., Rakhshaee, R., Radaee, A., & Heidarian, S. (2010). Catalytic reduction of methylene blue by sulfide ions in the presence of nanoAlMCM-41 material. Superlattices and Microstructures, 47(3), 411-421.

Srivastav, A. L., & Ranjan, M. (2020). Inorganic water pollutants Inorganic Pollutants in Water (pp. 1-15): Elsevier.

Sun, B., Li, H., Li, X., Liu, X., Zhang, C., Xu, H., & Zhao, X. (2018). Degradation of organic dyes over fenton-like Cu_2O–Cu/C catalysts. Industrial & Engineering Chemistry Research, 57(42), 14011-14021.

Sun, H., Abdeta, A. B., Kuo, D.-H., Wu, Q., Guo, Y., Zelekew, O. A., . . . Chen, X. (2021). Activated carbon supported CuSnOS catalyst with an efficient catalytic reduction of pollutants under dark condition. Journal of Molecular Liquids, 334, 116079.

Sun, H., Abdeta, A. B., Zelekew, O. A., Guo, Y., Zhang, J., Kuo, D.-H., . . . Chen, X. (2020). Spherical porous SiO_2 supported CuVOS catalyst with an efficient catalytic reduction of pollutants under dark condition. Journal of Molecular Liquids, 313, 113567.

Sun, H., Zelekew, O. A., Chen, X., Guo, Y., Kuo, D.-H., Lu, Q., & Lin, J. (2019a). A noble bimetal oxysulfide Cu V OS catalyst for highly efficient catalytic reduction of 4-nitrophenol and organic dyes. RSC Advances, 9(55), 31828-31839.

Sun, H., Zelekew, O. A., Chen, X., Guo, Y., Kuo, D.-H., Lu, Q., & Lin, J. (2019b). A noble bimetal oxysulfide CuVOS catalyst for highly efficient catalytic reduction of 4-nitrophenol and organic dyes. RSC Advances, 9(55), 31828-31839. doi:10.1039/C9RA05172D

Swathi, T., & Buvaneswari, G. (2008). Application of $NiCo_2O_4$ as a catalyst in the conversion of p-nitrophenol to p-aminophenol. Materials Letters, 62(23), 3900-3902.

Tadesse, S. F., Kuo, D.-H., Kebede, W. L., & Duresa, L. W. (2020a). Synthesis and characterization of vanadium-doped Mo $(O, S)_2$ oxysulfide for efficient photocatalytic degradation of organic dyes. New Journal of Chemistry, 44(45), 19868-19879.

Tadesse, S. F., Kuo, D.-H., Kebede, W. L., & Duresa, L. W. (2020b). Synthesis and characterization of vanadium-doped $Mo(O,S)_2$ oxysulfide for efficient photocatalytic degradation of organic dyes. New Journal of Chemistry, 44(45), 19868-19879. doi:10.1039/D0NJ02565H

Tadesse, S. F., Kuo, D.-H., Kebede, W. L., & Wolde, G. S. (2021). Visible light driven Nd_2O_3/Mo $(S, O)_{3-x}\cdot$ $0.34H_2O$ heterojunction for enhanced photocatalytic degradation of organic pollutants. Applied Surface Science, 569, 151091.

Taibi, M., Ammar, S., Jouini, N., Fiévet, F., Molinié, P., & Drillon, M. (2002). Layered nickel hydroxide salts: synthesis, characterization and magnetic behaviour in relation to the basal spacing. Journal of Materials Chemistry, 12(11), 3238-3244.

Tang, Q., Li, H., Zhang, J., Lin, Z., Pan, Y., Hu, Q., . . . Ye, Y. (2017). A dual-faced interlayer prepared by electron beam evaporation for enhanced-performance lithium–sulfur batteries. RSC Advances, 7(70), 44035-44042.

Tchangbedji, G., Odink, D., & Ouvrard, G. (1993). V_2O_4S—a new transition metal oxysulfide as positive for lithium batteries. Journal of power sources, 44(1-3), 577-581.

Tian, M., Dong, C., Cui, X., & Dong, Z. (2016). Nickel and cobalt nanoparticles modified hollow mesoporous carbon microsphere catalysts for efficient catalytic reduction of widely used dyes. RSC Advances, 6(101), 99114-99119.

Tran, P. D., Nguyen, M., Pramana, S. S., Bhattacharjee, A., Chiam, S. Y., Fize, J., . . . Loo, J. (2012). Copper molybdenum sulfide: a new efficient electrocatalyst for hydrogen production from water. Energy & Environmental Science, 5(10), 8912-8916.

Uppal, H., Chawla, S., Joshi, A. G., Haranath, D., Vijayan, N., & Singh, N. (2019). Facile chemical synthesis and novel application of zinc oxysulfide nanomaterial for instant and superior adsorption of arsenic from water. Journal of cleaner production, 208, 458-469.

Védrine, J. C. (2019). Metal oxides in heterogeneous oxidation catalysis: State of the art and challenges for a more sustainable world. ChemSusChem, 12(3), 577-588.

Veerakumar, P., Chen, S.-M., Madhu, R., Veeramani, V., Hung, C.-T., & Liu, S.-B. (2015). Nickel nanoparticle-decorated porous carbons for highly active catalytic reduction of organic dyes and sensitive detection of Hg (II) ions. ACS Applied Materials & Interfaces, 7(44), 24810-24821.

Wang, J., Wang, H., Yang, S., Tian, H., Liu, Y., Hao, Y., . . . Sun, B. (2018). A fluorescent probe for sensitive detection of hydrazine and its application in red wine and water. Analytical Sciences, 34(3), 329-333.

Wang, K., Ye, Y.-X., Jiang, C.-Y., Guo, M.-Y., Zhang, X.-Y., Jiang, A.-Q., . . . Zhu, H.-L. (2021). Design and synthesis of a novel “turn-on” fluorescent probe based on benzofuran-3 (2H)-one for detection of hydrazine in water samples and biological systems. Dyes and Pigments, 194, 109587.

Wang, Q., Nakabayashi, M., Hisatomi, T., Sun, S., Akiyama, S., Wang, Z., . . . Yamada, T. (2019). Oxysulfide photocatalyst for visible-light-driven overall water splitting. Nature materials, 18(8), 827-832.

Wang, X., Xiao, R., Li, H., & Chen, L. (2017). Oxysulfide LiAlSO: a lithium superionic conductor from first principles. Physical Review Letters, 118(19), 195901.

Wang, Y., Jiang, F., Chen, J., Sun, X., Xian, T., & Yang, H. (2020). In situ construction of CNT/CuS hybrids and their application in photodegradation for removing organic dyes. Nanomaterials, 10(1), 178.

Wasewar, K. L., Singh, S., & Kansal, S. K. (2020). Process intensification of treatment of inorganic water pollutants Inorganic Pollutants in Water (pp. 245-271): Elsevier.

Wu, H.-Y., Xie, Y.-L., & Hu, Z.-A. (2013). Synthesis, characterization and electrochemical properties of board-like Al-substituted alpha nickel hydroxides. Int. J. Electrochem. Sci, 8, 1839.

Wu, Q., Abdeta, A. B., Kuo, D.-H., Zhang, H., Lu, Q., Zhang, J., . . . Chen, X. (2022). A molybdenum sulfo-oxide/cobalt oxysulfide Z-scheme heterojunction catalyst for efficient photocatalytic hydrogen production and pollutant reduction. Journal of Materials Chemistry A, 10(10), 5328-5349.

Wu, Q., Wang, X., Fu, J., Zelekew, O. A., Abdeta, A. B., Kuo, D.-H., . . . Chen, X. (2021). Wool-coiled bimetallic oxysulfide MoSrOS catalyst synthesis for catalytic reduction of toxic organic pollutants and heavy metal ions. Journal of Science: Advanced Materials and Devices.

Wu, Y. (2017). The removal of methyl orange by periphytic biofilms: equilibrium and kinetic modeling. Periphyton. Functions and application in environmental remediation. Elsevier, 367-387.

Xia, Y., Liu, Y., Shi, N., & Zhang, X. (2019). Highly efficient reduction of 4-nitrophenolate to 4-aminophenolate by Au/γ-Fe $_2O_3$@ HAP magnetic composites. RSC Advances, 9(18), 10272-10281.

Xu, K., Zhang, B. Y., Mohiuddin, M., Ha, N., Wen, X., Zhou, C., . . . Zavabeti, A. (2021). Free-standing ultra-thin Janus indium oxysulfide for ultrasensitive visible-light-driven optoelectronic chemical sensing. Nano Today, 37, 101096.

Xue, Q., Pei, Z., Huang, Y., Zhu, M., Tang, Z., Li, H., . . . Zhi, C. (2017). Mn_3O_4 nanoparticles on layer-structured Ti_3C_2 MXene towards the oxygen reduction reaction and zinc–air batteries. Journal of Materials Chemistry A, 5(39), 20818-20823.

Yao, Y., Zhang, J., Chen, H., Yu, M., Gao, M., Hu, Y., & Wang, S. (2018). Ni0 encapsulated in N-doped carbon nanotubes for catalytic reduction of highly toxic hexavalent chromium. Applied Surface Science, 440, 421-431.

Yuan, Y.-J., Chen, D., Yu, Z.-T., & Zou, Z.-G. (2018). Cadmium sulfide-based nanomaterials for photocatalytic hydrogen production. Journal of Materials Chemistry A, 6(25), 11606-11630.

Yue, D., Qian, X., Ren, M., Fang, M., Jia, J., & Zhao, Y. (2018). Secondary battery inspired α-nickel hydroxide as an efficient Ni-based heterogeneous catalyst for sulfate radical activation. Science Bulletin, 63(5), 278-281.

Yufit, V., Nathan, M., Golodnitsky, D., & Peled, E. (2003). Thin-film lithium and lithium-ion batteries with electrochemically deposited molybdenum oxysulfide cathodes. Journal of power sources, 122(2), 169-173.

Zagklis, D. P., Koutsoukos, P. G., & Paraskeva, C. A. (2012). A combined coagulation/flocculation and membrane filtration process for the treatment of paint industry wastewaters. Industrial & Engineering Chemistry Research, 51(47), 15456-15462.

Zeleke, M. A., & Kuo, D.-H. (2019). Synthesis of oxy-sulfide based nanocomposite catalyst for visible light-driven reduction of Cr (VI). Environmental research, 172, 279-288.

Zeleke, M. A., Kuo, D.-H., Ahmed, K. E., & Gultom, N. S. (2018). Facile synthesis of bimetallic (In, Ga) 2 (O, S) 3 oxy-sulfide nanoflower and its enhanced photocatalytic activity for reduction of Cr (VI). Journal of colloid and interface science, 530, 567-578.

Zelekew, O. A., & Kuo, D.-H. (2017a). Facile synthesis of SiO2@ CuxO@ TiO2 heterostructures for catalytic reductions of 4-nitrophenol and 2-nitroaniline organic pollutants. Applied Surface Science, 393, 110-118.

Zelekew, O. A., & Kuo, D.-H. (2017b). Synthesis of a hierarchical structured NiO/NiS composite catalyst for reduction of 4-nitrophenol and organic dyes. RSC Advances, 7(8), 4353-4362.

Zelekew, O. A., Kuo, D.-H., & Abdullah, H. (2019). Synthesis of (Sn, Zn)(O, S) bimetallic oxysulfide catalyst for the detoxification of Cr^{+6} in aqueous solution. Advanced Powder Technology, 30(12), 3099-3106.

Zhang, J., Yu, J., Zhang, Y., Li, Q., & Gong, J. R. (2011). Visible light photocatalytic H2-production activity of CuS/ZnS porous nanosheets based on photoinduced interfacial charge transfer. Nano letters, 11(11), 4774-4779.

Zhang, L., Yang, X., Zhou, R., Lin, S., & Zhou, L. (2022). High-efficiency carbamazepine degradation using a Ni/Co-LDH as the peroxymonosulfate activator: Performance, mechanism and degradation pathway. Applied Surface Science, 574, 151580.

Zhang, X.-Y., Yang, Y.-S., Wang, W., Jiao, Q.-C., & Zhu, H.-L. (2020). Fluorescent sensors for the detection of hydrazine in environmental and biological systems: Recent advances and future prospects. Coordination Chemistry Reviews, 417, 213367.

Zhang, Y., Wang, X., Hu, D., Xue, C., Wang, W., Yang, H., . . . Wu, T. (2018). Monodisperse ultrasmall manganese-doped multimetallic oxysulfide nanoparticles as highly efficient oxygen reduction electrocatalyst. ACS Applied Materials & Interfaces, 10(16), 13413-13424.

Zhang, Z., Huo, H., Wang, L., Lou, S., Xiang, L., Xie, B., . . . Yin, G. (2021). Stacking fault disorder induced by Mn doping in Ni $(OH)_2$ for supercapacitor electrodes. Chemical Engineering Journal, 412, 128617.

Zhao, X., Niu, C., Zhang, L., Guo, H., Wen, X., Liang, C., & Zeng, G. (2018). Co-Mn layered double hydroxide as an effective heterogeneous catalyst for degradation of organic dyes by activation of peroxymonosulfate. Chemosphere, 204, 11-21.

Zheng, L., Teng, F., Ye, X., Zheng, H., & Fang, X. (2020). Photo/electrochemical applications of metal sulfide/TiO_2 heterostructures. Advanced Energy Materials, 10(1), 1902355.

Zheng, Y., Sun, L., Liu, W., Wang, C., Dai, Z., & Ma, F. (2020). Tungsten oxysulfide nanosheets for highly sensitive and selective NH 3 sensing. Journal of Materials Chemistry C, 8(12), 4206-4214.

Zhou, H., Xu, K., Ha, N., Cheng, Y., Ou, R., Ma, Q., . . . Ou, J. Z. (2022). Reversible Room Temperature H2 Gas Sensing Based on Self-Assembled Cobalt Oxysulfide. Sensors, 22(1), 303.

Zhu, B., & Scanlon, D. O. (2022). Predicting Lithium Iron Oxysulfides for Battery Cathodes. ACS Applied Energy Materials.

Zhu, J., Chen, C., Li, Y., Zhou, L., & Lan, Y. (2019). Rapid degradation of aniline by peroxydisulfate activated with copper-nickel binary oxysulfide. Separation and Purification Technology, 209, 1007-1015.

Zhu, J., Tang, S., Xie, H., Dai, Y., & Meng, X. (2014). Hierarchically porous MnO2 microspheres doped with homogeneously distributed Fe_3O_4 nanoparticles for supercapacitors. ACS Applied Materials & Interfaces, 6(20), 17637-17646.

Zhu, M., Wang, C., Meng, D., & Diao, G. (2013). In situ synthesis of silver nanostructures on magnetic $Fe_3 O_4$@ C core–shell nanocomposites and their application in catalytic reduction reactions. Journal of Materials Chemistry A, 1(6), 2118-2125.

Research Fund Acknowledgement

This research thesis was funded by Adama Science and Technology University under the grant number of ASTU/SM-R/437/22, Adama, Ethiopia.